Repulsive versus attractive Hubbard model: Transport properties and spin-lattice relaxation rate

Rok Žitko,[1,2] Žiga Osolin,[1] and Peter Jeglič[1]
[1]*Jožef Stefan Institute, Jamova 39, SI-1000 Ljubljana, Slovenia*
[2]*Faculty of Mathematics and Physics, University of Ljubljana, Jadranska 19, SI-1000 Ljubljana, Slovenia*
(Received 15 December 2014; revised manuscript received 21 February 2015; published 8 April 2015)

We contrast the transport properties (dc resistivity, Seebeck coefficient), optical conductivity, spectral functions, dynamical magnetic susceptibility, and the nuclear magnetic resonance $1/T_1$ spin-lattice relaxation rate of the repulsive and attractive infinite-dimensional Hubbard models in the paramagnetic phase for a generic band filling. The calculations are performed in a wide temperature interval using the dynamical mean-field theory with the numerical renormalization group as the impurity solver. The attractive case exhibits significantly more complex temperature dependencies which can be explained by the behavior of the half-filled Hubbard model in external magnetic field with constant magnetization, to which the attractive Hubbard model maps through the partial particle-hole transformation. The resistivity is nonmonotonous for the strongly attractive case: it peaks significantly above the Mott-Ioffe-Regel value at a temperature $T_{\max}$ where the quasiparticle band disappears. For both signs of U we find particle-hole asymmetry in the self-energy at low energies, but with the opposite kind of excitations having longer lifetime. This leads to a strong suppression of the slope of the Seebeck coefficient in the attractive case rather than an enhancement as in the repulsive case. The spin-lattice relaxation rate in the strongly attractive case has a nonmonotonic temperature dependence, thereby revealing the pairing fluctuations.

DOI: 10.1103/PhysRevB.91.155111 PACS number(s): 71.27.+a, 71.30.+h, 72.15.Qm

I. INTRODUCTION

Electrons in materials are charged particles that repel each other through Coulomb interaction, but effective electron-electron attraction can be generated by coupling to lattice vibrations [1]. The Hubbard model [2–4] describes a lattice with a short-ranged (onsite) electron-electron interaction U which can be either positive (repulsion) or negative (attraction). The repulsive Hubbard model is a minimal model for the cuprate family of superconducting materials [5,6] and describes the competition between the delocalizing effects of electron hopping and localizing effects of charge repulsion. The attractive Hubbard model is used as an effective description for certain systems with very strong electron-phonon coupling and for cold atoms in optical lattices [7–9]. It has been used to study, for example, strong-coupling superconductors and the continuous crossover between the BEC and BCS superconducting regimes [10–16].

There are very few works that directly address the differences between the repulsive and the attractive regimes of the Hubbard model. While at the particle-hole-symmetric point (i.e., at half-filling, for one electron per lattice site), the two cases are trivially related by a partial particle-hole transformation that leads to $U \to -U$ and simply exchanges the spin and charge sectors, this is no longer the case at finite doping since the doping corresponds to the magnetization under this mapping. Comparative studies of repulsive and attractive Hubbard models are very valuable for understanding more complex models such as the Hubbard-Holstein model [17–20], where for increasing electron-phonon (e-ph) coupling the effective electron-electron (e-e) interaction becomes attractive on low-energy scales, while remaining repulsive at higher energies. They are also of interest in the context of fermionic cold atoms trapped in optical lattices [21], where the strength and even the sign of the interaction can be tuned by means of Feshbach resonances. In this work, we study the paramagnetic phase of the Hubbard model at moderate hole doping $\langle n \rangle = 0.8$ for both signs of U using the dynamical mean-field theory (DMFT) [22,23]. Magnetic order, charge-density-wave, and superconducting DMFT solutions are also possible [11–13,15,24–27], but not considered in our calculations. In other words, we only consider the paramagnetic (nonmagnetic, normal-state) phase that is uniform in space. Even if the true ground state is actually ordered, our results are still valid above the ordering temperature [11–13,28]. Furthermore, since the ordering temperatures can be significantly reduced by frustration (such as that due to the next-nearest-neighbor hopping or external magnetic field), the range of qualitative validity of our results can extend to very low temperatures in such cases [11,13].

We focus on the experimentally most relevant properties: transport (resistivity and Seebeck coefficient), optical conductivity, and NMR $1/T_1$ spin-lattice relaxation rate as a function of temperature, but we also provide results for thermodynamics, spectral functions, and dynamical spin susceptibility. The main results of this work concern the attractive Hubbard model: (a) identification of the characteristic energy scales, (b) opposite signs of the particle-hole asymmetry of velocities and scattering rate, leading to a near cancellation of the contributions to the low-temperature Seebeck coefficient, and (c) the nonmonotonic temperature dependence of the spin-lattice relaxation rate.

This work is structured as follows. In Sec. II, we introduce the model and discuss the partial particle-hole transformation. In Sec. III, we describe the thermodynamic properties as a function of Hubbard coupling U and temperature T. In Sec. IV, we discuss the local and momentum-resolved spectral functions, the U dependence of the quasiparticle renormalization factor Z, and the asymmetric structure of the self-energy Σ and its temperature variation. In Sec. V, we describe the transport properties and provide some details about the nonmonotonous temperature dependencies in the attractive Hubbard model. In Sec. VII, we compare the spin-lattice relaxation rates and discuss the temperature

dependence of the dynamical susceptibilities. Section VIII is devoted to the DMFT mapping in the attractive-U case, where the effective model is the particle-hole-symmetric Anderson impurity model at constant magnetization and we discuss to what degree the properties of the impurity model reflect in the fully self-consistent DMFT calculations. Finally, Sec. IX concerns the experimental relevance of our calculations and presents some additional results for the optical conductivity that could aid in the interpretation of the measurements on zeolite materials.

II. MODEL AND METHOD

We study the Hubbard model

$$H = \sum_{\mathbf{k}\sigma} \epsilon_{\mathbf{k}} c^{\dagger}_{\mathbf{k}\sigma} c_{\mathbf{k}\sigma} + U \sum_{i} n_{i\uparrow} n_{i\downarrow}. \tag{1}$$

$\epsilon_{\mathbf{k}}$ is the dispersion relation of electrons with wave vector $\mathbf{k}$ and spin σ, U is the Hubbard coupling. Index i ranges over all lattice sites, while $n_{i\sigma} = c^{\dagger}_{i\sigma} c_{i\sigma}$.

We seek a nonordered solution of this model using the DMFT [22,23,29]. In this approach, the bulk problem defined on the lattice maps onto a quantum impurity model (here the single-impurity Anderson model) subject to a self-consistency condition for the hybridization function [24,30–32]. This technique takes into account all local quantum fluctuations exactly, while the intersite correlations are treated at the static mean-field level. This is a good approximation for problems where the most important effects are local in nature (Mott metal-insulator transition, etc.). It is an exact method in the limit of infinite dimensions or infinite lattice connectivity, and appears to be reasonably reliable as an approximative technique for three-dimensional (3D) lattices [23,33], while for two- (2D) and one-dimensional (1D) systems it is less applicable due to stronger nonlocal fluctuations.

We work with the Bethe lattice that has noninteracting density of states (DOS)

$$\rho_0(\epsilon) = \frac{2}{\pi D} \sqrt{1 - (\epsilon/D)^2}, \tag{2}$$

which mimics some of the features of the 3D cubic lattice DOS, in particular, the square-root band-edge singularities. D is the half-bandwidth that we use to express the parameters and the results as dimensionless quantities.

As the impurity solver, we use the numerical renormalization group (NRG) [34–42] with discretization parameter $\Lambda = 2$, twist averaging over $N_z = 16$ values [43,44], and keeping up to 12 000 multiplets (or up to a truncation cutoff at energy $10\omega_N$, where ω_N is the characteristic energy at the Nth NRG step). The twist averaging in the NRG means that N_z separate NRG calculations are run for different choices of interleaved discretization grids (so-called z parameters) and the results are then averaged; this technique leads to a significant cancellation of the discretization artifacts of the method. Spectral broadening has been performed with parameter $\alpha = 0.3$. We use Broyden's method to speed up the convergence of the DMFT iteration and to control the chemical potential in the constant-occupancy calculations [45]. The convergence criteria are very stringent (integrated absolute value of the difference of spectral functions less than 10^{-8}) in an attempt to obtain reliable results for transport properties at low temperatures. In spite of these efforts, the residual oscillatory features in the self-energy remain problematic at low temperatures; for computing transport properties, it is necessary to perform fitting of the self-energy with low-order polynomials around $\omega = 0$. In particular, the results for the Seebeck coefficient turn out to be exceedingly difficult to compute reliably at very low temperatures.

On bipartite lattices the repulsive and the attractive Hubbard models are related through the partial particle-hole (Lieb-Mattis) transformation [7,12,13,46] defined as

$$c^{\dagger}_{i\uparrow} \to d^{\dagger}_{i\uparrow}, \quad c^{\dagger}_{i\downarrow} \to (-1)^i d_{i\downarrow}. \tag{3}$$

For down spins, this can be interpreted as a mapping of the particle creation operators onto the annihilation operators for the holes. The $(-1)^i$ factor indicates different prefactors for the two sublattices of a bipartite lattice. The transformation leaves the kinetic energy unchanged, but changes the sign of the quartic electron-electron coupling term, i.e., flips the sign of U. Furthermore, it can be seen that the particle-number (density) operator for c particles maps onto the spin-z (magnetization) operator for d particles. While the spin-up Green's function is invariant, the spin-down Green's function is transformed. Since $\langle\langle A; B\rangle\rangle_z = -\langle\langle B; A\rangle\rangle_{-z}$, the transformation is

$$A_{i\downarrow}(\omega) \to A_{i\downarrow}(-\omega). \tag{4}$$

This implies that the field-induced Zeeman splitting of the quasiparticle band in the $U > 0$ case corresponds to a uniform shift of the quasiparticle band through changes of the chemical potential in the $U < 0$ case. This has important consequences for the transport properties, especially for the Seebeck coefficient which is sensitive to the particle-hole asymmetry.

Unless noted otherwise, the band filling is $\langle n\rangle = 0.8$, i.e., the hole doping level is $\delta = 1 - \langle n\rangle = 0.2$, which is sufficiently away from any special points to be considered as a generic band filling. For attractive U, similar DMFT studies have been performed using different impurity solvers (Hirsch-Fye QMC, exact diagonalization), focusing on the pairing transition in the paramagnetic case [11,12] and on the superconducting solution [13]. The advantage of the NRG compared to those works is in the higher spectral resolution and large temperature range of applicability, from $T = 0$ to temperatures comparable to the bandwidth. Some results for the attractive U computed using the DMFT(NRG) approach have recently been reported [16].

The attractive Hubbard model on the infinite-connectivity Bethe lattice (and more generally on bipartite lattices in dimension higher than two) has a superconducting solution for all U and all densities n [10]. If the superconductivity is suppressed, the normal state is a Fermi liquid (metallic) for $U > U_0$ and a bound-pair (insulating) state for $U < U_0$, separated by a pairing quantum phase transition at U_0 which is equivalent to the Mott metal-insulator transition in the presence of the magnetic field for the $U > 0$ model [11–13,23,47–50]. For finite doping, it has been shown that the transition is first order [12].

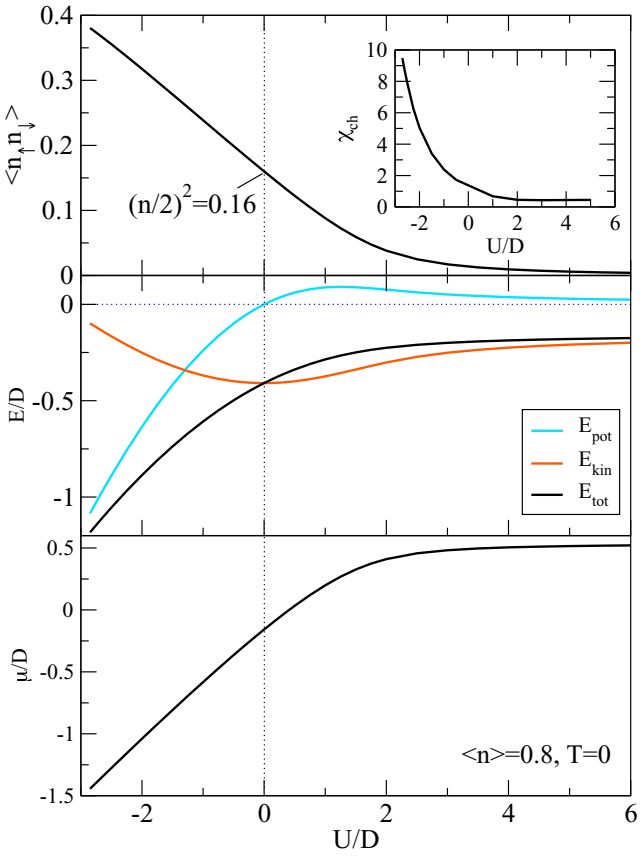

FIG. 1. (Color online) Zero-temperature thermodynamic properties of the Hubbard model as a function of the electron-electron interaction parameter U. The density is fixed at $n = 0.8$. (a) Double occupancy (density of doubly occupied sites) $P_2 = \langle n_\uparrow n_\downarrow \rangle$. The inset shows the uniform charge susceptibility $\chi_c = \partial\langle n\rangle/\partial\mu$. The temperature dependence of P_2 is shown in Fig. 15. (b) Potential, kinetic, and total energy per particle. (c) Chemical potential.

III. THERMODYNAMIC PROPERTIES

We first consider the static (thermodynamic) properties. In Fig. 1(a), we show the double occupancy $P_2 = \langle n_\uparrow n_\downarrow \rangle$, which is a measure of local pair formation [11]. The noninteracting result at $U = 0$, $(n/2)^2 = 0.16$ is rapidly reduced for repulsive U with maximum curvature in the range where the upper Hubbard band emerges ($U \approx 2D$, see Fig. 4) and tends to zero as $1/U$ in the large-U limit. For attractive U, the double occupancy at zero temperature increases with increasing $|U|$ up to values close to $n/2 = 0.4$, at which point the constant-occupancy DMFT calculations no longer converge due to a very high charge susceptibility close to the pairing phase transition (see the inset in Fig. 1) and the coexistence of several solutions of the DMFT equations [12]. Asymptotically, in the pairing phase, one would expect that all particles are bound as local pairs for infinite attraction, so that $P_2 \to n/2 = 0.4$ when $U \to -\infty$. In the parameter range where P_2 becomes large and the convergence slow, it helps to perform the DMFT calculations at a fixed chemical potential μ and determine the appropriate μ by bisection; this becomes crucial in the parameter range where there is a phase separation. The instability also manifests itself as a large

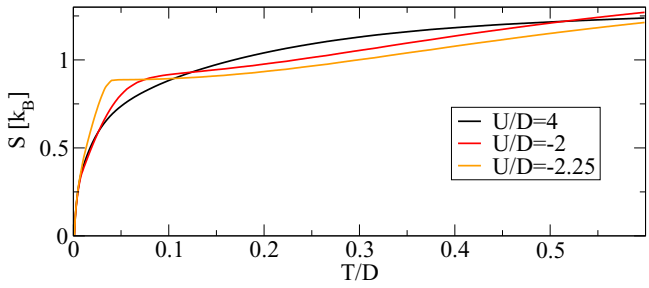

FIG. 2. (Color online) Temperature dependence of entropy per lattice site for a set of U values.

spread of the expectation values of physical observables in the z-averaging method in the NRG calculations. For example, at $U/D = -2.85$, the computed $\langle n\rangle$ values range from 0.741 to 0.861 for different discretization grids, thus the quantitative validity of the results becomes questionable (for comparison, generally the differences between $\langle n\rangle$ are of order 10^{-4}). Such behavior is a well-known precursor of phase transitions in the NRG calculations. The NRG calculations using the twist averaging must, namely, be performed with caution close to quantum phase transitions, since for different values of z the system may be in different phases, thus the z averaging itself becomes meaningless. The severity of this problem depends on the system and on the type of the transition. For the attractive Hubbard model constrained to the normal phase, as studied here, the difficulties are particularly strong. Therefore, using the DMFT(NRG) approach, it is difficult to locate the transition point and to study its nature.[1]

In Fig. 1(b), we follow the kinetic and potential energies. The potential energy is given simply by $U\langle n_\uparrow n_\downarrow\rangle$, thus it does not bring any new information. $E_{\rm kin}$ is minimal in the noninteracting case. It increases for both signs of U because interactions of both signs lead to increased particle localization which costs kinetic energy.

We now consider the temperature dependence of the entropy. In Fig. 2, we show representative cases for strongly repulsive and strongly attractive interaction. For both signs of U, the entropy attains values of order $\ln 2 \approx 0.69$ already at relatively low temperatures. This indicates the presence of fluctuating local moments (for repulsive U, i.e., a bad metal regime of doped Mott insulators) or paired states (attractive U, i.e., an incoherent pairing state). The entropy curves for attractive U have a pronounced plateau at intermediate temperatures. For example, at $U/D = -2.25$ the low-temperature nearly linear region is followed by a plateau starting at $T = T_{\rm pl} \approx 0.04D$, up to $T \approx 0.1D$ at which point it starts to gradually rise again. The temperature scale $T_{\rm pl}$ is also visible in the chemical potential $\mu(T)$: for $T < T_{\rm pl}$, the chemical potential is nearly constant,

[1] One way to proceed is to perform the NRG calculation for different values of z *without* averaging the results, thus obtaining different transition points for the different values of z. The true transition occurs at the average of the z-dependent values. In addition, in such cases it becomes important to consider the dependence of the results on the discretization parameter Λ and the approach to the continuum limit $\Lambda \to 1$.

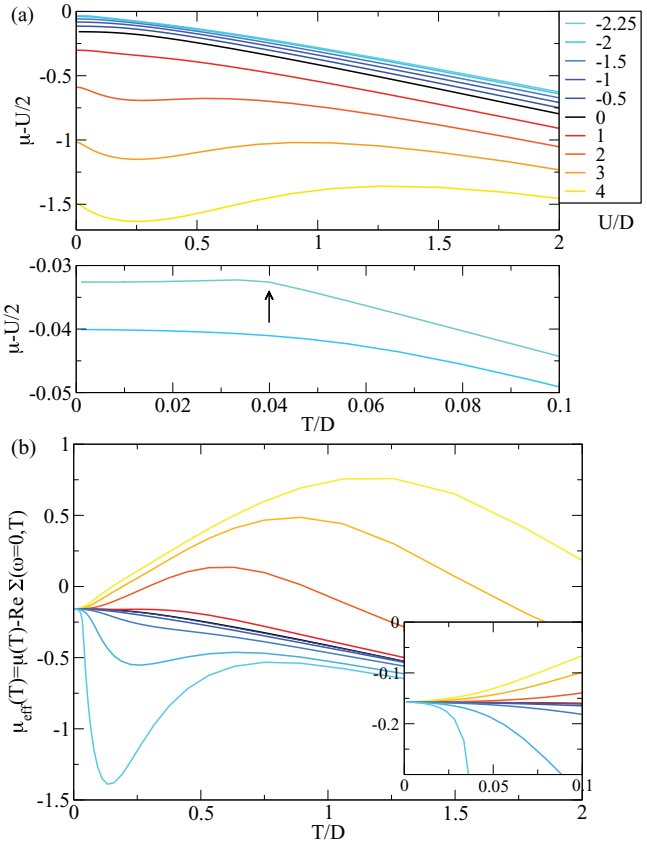

FIG. 3. (Color online) (a) Temperature dependence of the chemical potential (shifted by $-U/2$). The zero-temperature values of the chemical potential (without the shift) are also shown in Fig. 1(c). (b) Temperature dependence of the renormalized chemical potential $\mu_{\rm eff}(T) = \mu(T) - {\rm Re}\Sigma(\omega = 0, T)$.

then it rapidly crosses over into a new decreasing regime that smoothly connects with the asymptotic linear behavior (see Fig. 3). At $T_{\rm pl}$, the quasiparticle band is already reduced, but not yet fully eliminated.

We note that under the $U \to -U$ mapping, the chemical potential corresponds to the magnetic field required to maintain the magnetization constant. In the following, we show that the plateau starting at $T_{\rm pl}$ can be related to features seen in the double occupancy, dynamical susceptibility, and spin-lattice relaxation curves, but not so well in the transport properties. It indicates the regime where the electron pairing interaction tends to eliminate the coherent Fermi-liquid state.

In Fig. 3(b), we show the temperature dependence of the renormalized chemical potential defined as

$$\mu_{\rm eff}(T) = \mu(T) - {\rm Re}\Sigma(\omega = 0, T). \tag{5}$$

This quantity determines the location of the peak in the momentum distribution curves $A(\epsilon, \omega = 0)$. At $T = 0$, its value is fixed by the Luttinger theorem to the noninteracting Fermi level. For strong interaction of either sign, the renormalized chemical potential deviates strongly from the $U = 0$ result already at very low temperatures on the scale of T_F. For the repulsive interaction, as the temperature increases the Fermi volume first expands [51] (in the sense that the peak in the momentum distribution shifts to higher ϵ at higher temperatures), while for the attractive interaction it *contracts*. This provides a simple picture: the repulsive interaction tends to expand the Fermi sphere upon heating (electrons reduce double occupancy of the occupied ϵ_k levels), while the attractive interaction contracts it (electrons increase double occupancy of the occupied ϵ_k levels); this is also confirmed by the temperature dependence of pairing, shown in Fig. 15(b). For repulsive interaction, this trend continues to high temperatures and reverses on a scale determined by U where the system approaches the atomic limit. For attractive interaction, the Fermi surface contraction terminates on an intermediate temperature scale of order ZD; this is followed up by a region of increasing $\mu_{\rm eff}$ until the final approach to the atomic limit where $\mu_{\rm eff}$ is decreasing.

IV. SINGLE-PARTICLE DYNAMICAL PROPERTIES

A. Zero-temperature spectral functions

In the DMFT, the lattice (momentum-resolved) Green's function is approximated using a self-energy function that depends only on the frequency but not on the momentum, so that

$$G_{\mathbf{k}}(z) = \frac{1}{z + \mu - \epsilon_{\mathbf{k}} - \Sigma(z)}, \tag{6}$$

where z is complex frequency (one may take $z = \omega + i\delta$ to obtain the retarded Green's function). The local Green's function is obtained as the $\mathbf{k}$ average:

$$\begin{aligned} G_{\rm loc}(z) &= \frac{1}{N}\sum_{\mathbf{k}} G_{\mathbf{k}}(z) = \int \frac{\rho_0(\epsilon)\, d\epsilon}{z + \mu - \epsilon - \Sigma(z)} \\ &= G_0[z + \mu - \Sigma(z)], \end{aligned} \tag{7}$$

where N is the number of lattice sites and $G_0(z)$ is the noninteracting Green's function of the chosen lattice, here

$$G_0(z) = \frac{2}{D}(z/D - {\rm sign}[{\rm Im}(z)]\sqrt{1 - (z/D)^2}). \tag{8}$$

Momentum-resolved and local spectral functions are then defined as $A_{\mathbf{k}}(\omega) = (-1/\pi){\rm Im}G_{\mathbf{k}}(\omega + i\delta)$ and $A(\omega) = (-1/\pi){\rm Im}G_{\rm loc}(\omega + i\delta)$.

In Figs. 4(a) and 4(b), we compare the local spectral functions $A(\omega)$ for both signs of U. For positive U, as U increases the upper and lower Hubbard bands emerge and there is a narrow quasiparticle (QP) band at the Fermi level. For very large U, the low-energy part of the spectrum no longer changes, while the upper Hubbard band shifts to higher energies [52]. In the large-U regime, the system is a doped Mott insulator, which is a Fermi liquid at low temperatures and a bad metal at high temperatures [51].

For negative U, the local spectral function also features Hubbard bands and a QP peak, but the evolution as a function of U is quite different. This problem maps onto the half-filled repulsive Hubbard band in the presence of an external magnetic field of such intensity that the magnetization remains constant. With increasing $|U|$, the low-energy scale (Kondo temperature) is reduced exponentially, thus the QP band shrinks. The negative-U model corresponds to the $B \sim T_K$ regime in the language of the effective quantum impurity model with positive U. This is precisely the nontrivial

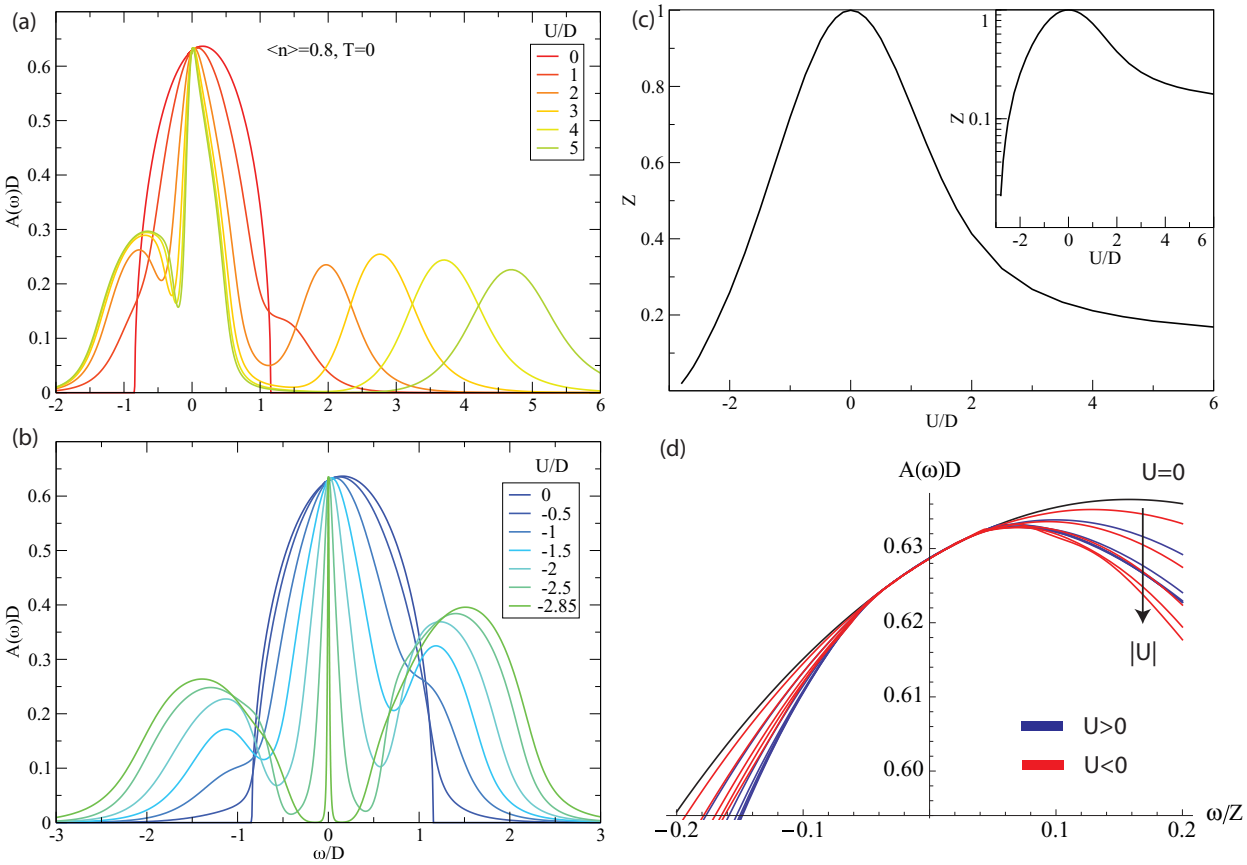

FIG. 4. (Color online) Local spectral function $A(\omega)$ at zero temperature for (a) repulsive and (b) attractive cases. (c) Quasiparticle renormalization factor $Z \equiv Z(T=0)$ as a function of U. (d) Low-frequency part of the spectral function rescaled as $A(\omega/Z)$. We plot the results for $U = -2.5,-2,-1.5,-1,-0.5,0,1,2,3,4,5,6D$.

crossover regime between the well-understood $B = 0$ Kondo limit and the noninteracting $B \to \infty$ limit [48,53]. The position of the Hubbard bands is rather symmetric with respect to zero frequency, but we note the difference in the weight which corresponds to doping in the $U < 0$ picture (or to finite magnetization in the half-filled effective $U > 0$ model picture).

In Fig. 4(c), we plot the quasiparticle renormalization factor

$$Z(T) = \left(1 - \mathrm{Re}\left[\frac{d\Sigma(\omega,T)}{d\omega}\right]_{\omega=0}\right)^{-1} \qquad (9)$$

at zero temperature $Z \equiv Z(T=0)$. It quantifies the renormalized mass $m^* = m/Z$ and the QP lifetime $\tau^* = Z\tau$.

If the argument of the spectral function is rescaled as ω/Z, we find that all spectral functions overlap well in the interval $-0.05 \lesssim \omega/Z \lesssim 0.05$. For the positive-$U$ case, this corresponds to the fact that the Fermi-liquid regime extends up to $T_{\mathrm{FL}} \approx 0.05\delta D \approx 0.05ZD$ (see Refs. [51,52] and Sec. V). For the negative-U case, however, this scale ($0.05Z$) is not visible in the transport properties.

The temperature dependence of spectra for the attractive case is shown in Fig. 5, where we plot the momentum-resolved (ϵ-dependent) spectral functions. We observe the gradual disappearance of the QP band (finished by $T \approx 0.15D$), while the high-energy Hubbard bands are not affected much in this temperature range.

B. Self-energy and particle-hole asymmetry

We now compare the structure of the self-energy function in the repulsive and attractive cases. For weak interaction,

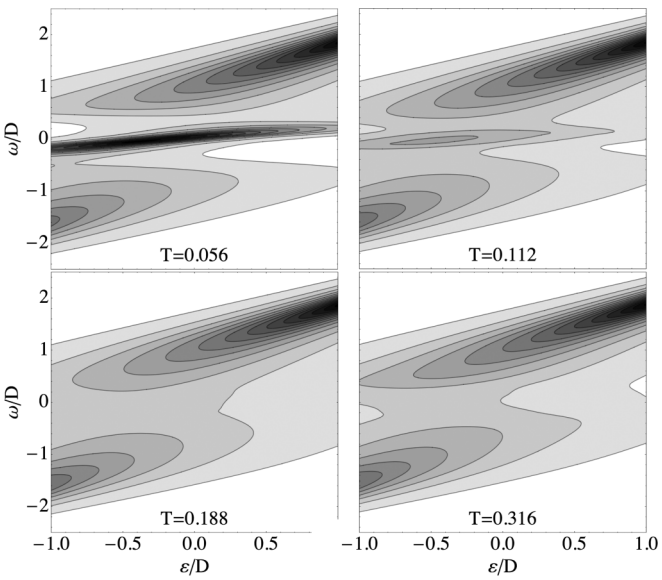

FIG. 5. Momentum-resolved spectral functions $A(\epsilon,\omega)$ for a range of temperatures for attractive interaction with $U/D = -2$.

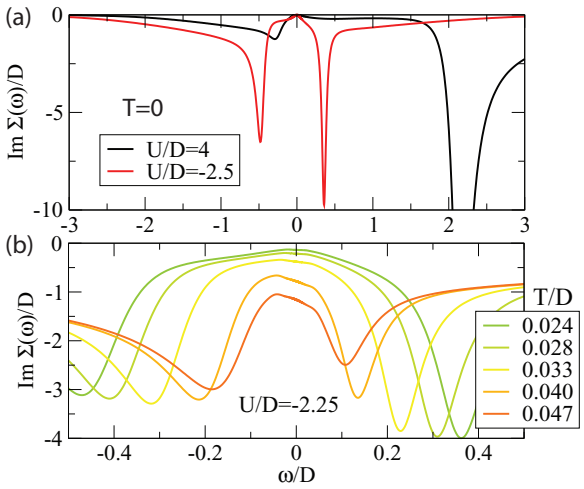

FIG. 6. (Color online) (a) Imaginary part of the self-energy at $T = 0$ for strongly repulsive and strongly attractive interactions reveals particle-hole asymmetry at low-energy scales in both cases. (b) Temperature dependence of $\mathrm{Im}\Sigma(\omega)$ for the attractive Hubbard model at $U/D = -2.25$.

they are qualitatively similar and can be reproduced using the perturbation theory: in $\mathrm{Im}\Sigma(\omega)$ there are two broad peaks centered approximately at $\omega = \pm|U|$. For strong interactions, the case shown in Fig. 6(a), the differences become more pronounced. The $U/D = 4$ case has been thoroughly studied recently in Ref. [51], where the strong particle-hole asymmetry in vicinity of the Fermi level has been pointed out. For strongly negative U, we also find asymmetry in the low-energy part, but in this case the plateau in $\mathrm{Im}\Sigma(\omega)$ is found on the *hole side* rather than on the particle side, and it is less pronounced. In a simplified picture where the asymmetry is related to the reduced density of states needed for scattering, the long-lived resilient quasiparticle states for $U > 0$ are due to displacement of the upper Hubbard band to high energies, while the long(er)-lived quasihole states for $U < 0$ are not related so much to the position of the lower Hubbard band, but rather to its lower spectral weight (compared with the symmetrically located upper Hubbard band).

For $U < 0$, the resonance structures in $\mathrm{Im}\Sigma$ remain rather sharp on both particle and hole sides; they tend toward small ω as $|U|$ increases, which reflects the structure of the spectral function with shrinking QP band (resonances in $\mathrm{Im}\Sigma$ follow from the analytical structure of the Green's functions and are expected between any two spectral peaks in single-orbital problems). For strongly attractive U, the asymmetry decreases for increasing $|U|$.

The temperature dependence of $\mathrm{Im}\Sigma(\omega)$ in the attractive case reveals an interesting reversal of the asymmetry [see Fig. 6(b)]. This is another nontrivial effect of the constant-magnetization constraint; it indicates that the $T = 0$ self-energy does not permit an easy identification of the transport mechanisms at elevated temperatures.

V. TRANSPORT PROPERTIES

In the DMFT, the vertex corrections drop out and the optical conductivity is fully determined by the self-energy alone [23,54–62]:

$$\mathrm{Re}\,\sigma(\omega) = \frac{2\pi e^2}{\hbar}\int d\omega'\, F(\omega,\omega')\int d\epsilon\, \Phi(\epsilon)A_\epsilon(\omega')A_\epsilon(\omega'+\omega), \tag{10}$$

with $F(\omega,\omega') = [f(\omega') - f(\omega+\omega')]/\omega$, where $f(\omega) = [1 + \exp(\beta\omega)]^{-1}$ is the Fermi function, $A_\epsilon(\omega) = -(1/\pi)\mathrm{Im}[\omega + \mu - \epsilon - \Sigma(\omega)]^{-1}$, and $\Phi(\epsilon)$ is the transport function defined through the derivatives of the dispersion relation

$$\Phi(\epsilon) = \frac{1}{V}\sum_k \left(\frac{d\epsilon_k}{dk}\right)^2 \delta(\epsilon - \epsilon_k). \tag{11}$$

The expression for $\mathrm{Re}\,\sigma(\omega)$ in Eq. (10) is valid generally for a single-band model defined on a lattice which is periodic and exhibits inversion symmetry in the direction of current [62]. The Bethe lattice is not a regular lattice and there is no notion of reciprocal space or momenta, thus there are ambiguities in the definition of the currents, the optical conductivity $\sigma(\omega)$, and the transport function $\Phi(\epsilon)$. We use $\Phi(\epsilon) = \Phi(0)[1 - (\epsilon/D)^2]^{3/2}$, which satisfies the f-sum rule [62–64]. The choice of $\Phi(\epsilon)$ has very little effect on the results for the resistivity. It affects the Seebeck coefficient more significantly, especially for negative U (where, however, S is small); this is discussed in more detail in Sec. V C. In most cases, however, the effects of Φ are quantitative, not qualitative.

A. Resistivity

We consider first the dc resistivity $\rho = 1/\sigma(0)$ at fixed low temperature as a function of the interaction strength U (see Fig. 7, top panel). The most notable feature is the rapid resistivity increase for large attraction $U \lesssim -2D$. This effect is much stronger than the growing resistivity for increasing repulsion for $U > 0$. This can be explained by the strong decrease of the effective Kondo temperature, and the corresponding decrease of the QP lifetime τ^* [see Fig. 4(c)].

In Fig. 8, we plot the temperature dependence of the transport properties. At low temperatures, we always find the Fermi-liquid behavior $\rho \propto T^2$ below some temperature T_{FL} for $U > U_0$. In the repulsive case, T_{FL} is given by $T_{\mathrm{FL}} \approx 0.05\delta D$ where δ is doping with respect to half-filling $\delta = 1 - \langle n\rangle$ [51]. For large positive U, the resistivity above T_{FL} increases linearly with negative intercept up to T^*, where the slope changes and the resistivity is linear with positive intercept [51]. In the attractive case, the quadratic dependence extends to much higher temperatures; for $U/D \gtrsim -2$, it goes essentially up to the maximum resistivity at approximately $T_{\mathrm{max}} = ZD$. For even stronger attraction, there is a clearer separation between the T_{FL} and T_{max} scales (see Fig. 9). Well-defined QP excitations survive almost up to the high-temperature scale T_{max}, similar to the resilient quasiparticles identified in the repulsive case which exist up to T_{MIR} where ρ reaches the Mott-Ioffe-Regel (MIR) value [51]. In the attractive case at T_{max}, the resistivity for large enough $|U|$ surpasses the Mott-Ioffe-Regel limit, thus resilient quasiparticles exist even in this regime.

While in the repulsive case the characteristic temperature scales T_{FL} and T_{MIR} are proportional to doping $\delta = 1 - \langle n\rangle$, in the attractive case the doping does not affect much the

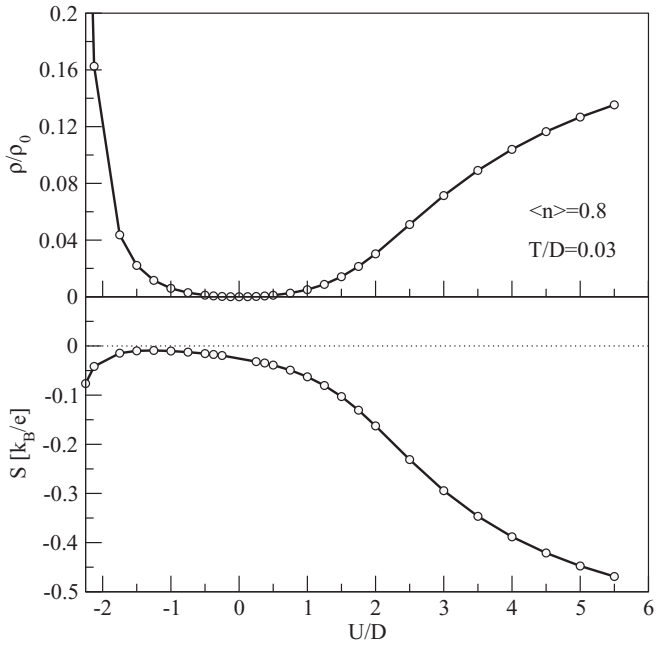

FIG. 7. Resistivity and Seebeck coefficient of the Hubbard model at constant temperature $T = 3 \times 10^{-2} D$. The resistivity is expressed in units of the Mott-Ioffe-Regel value $\rho_0 = (e^2/\hbar)\Phi(0)/D$. The results for the Seebeck coefficient for the values of U where the calculation is not reliable have been omitted.

resistivity curves which are almost overlapping (see Fig. 10). $T_{\max}$ depends mostly on U, while the doping controls the peak value of resistivity, but even this dependence is found to be very weak. These results can be explained by the trends seen in the spectral function at low temperature: the QP band is not affected much by the amount of doping (there is a minor shift of its low-energy edge, while the high-energy edge is almost invariant), while there is a significant reorganization of the spectral weight between the lower and the upper Hubbard bands at high frequencies (this reflects the changing magnetization in the language of the effective positive-U model at half-filling), but this has little effect on the resistivity on temperature scales sufficiently below $\sim|U|/2$.

B. Thermopower (Seebeck coefficient)

The thermopower (Seebeck coefficient) is defined as

$$S = -\frac{k_B}{e_0 T}\frac{L_{12}}{L_{11}}, \tag{12}$$

where the transport integrals in the infinite-d limit are given by [61]

$$L_{jk} = \int d\omega \left(-\frac{\partial f(\omega)}{\partial \omega}\right)\left[\sum_\sigma \int d\epsilon\, \Phi(\epsilon) A_{\sigma,\epsilon}(\omega)^2\right]^j \omega^{k-1}. \tag{13}$$

The results at the constant low temperature are shown in Fig. 7, bottom panel. The Seebeck coefficient for small U is negative because of the asymmetry of the transport function around the Fermi level (particle-hole asymmetry of electron velocities). For increasing interaction, it becomes

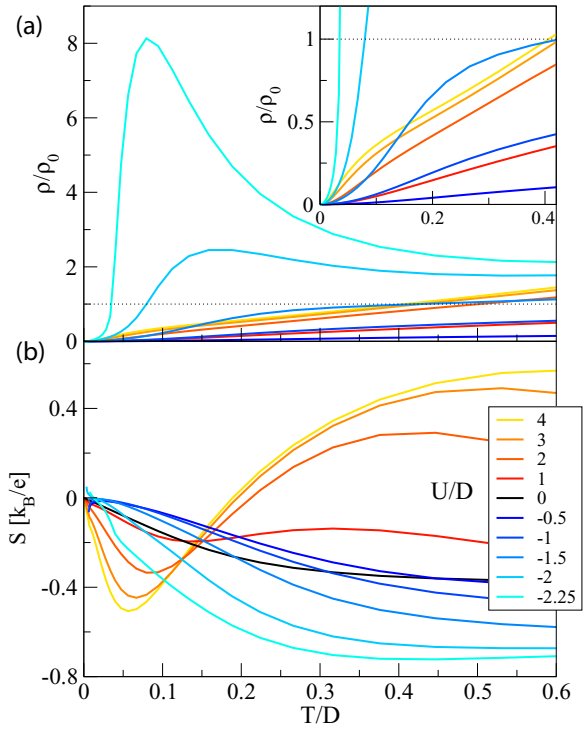

FIG. 8. (Color online) Temperature dependence of resistivity and Seebeck coefficient. ρ_0 is the MIR resistivity. We note that for even higher temperatures, not shown in the plot, the resistivity for $U/D = -2$ and $U/D = -2.25$ starts to increase, i.e., there appears to be no saturation of resistivity for either sign of U. At very low temperatures (for $T/D \lesssim 0.01$), the results for the Seebeck coefficient become unreliable due to increasing error in dividing two small values of the transport integrals L_{12} and L_{11}, but also due to the intrinsic problems of the NRG method in the calculations of the self-energy function at very small energies and temperatures (causality violations).

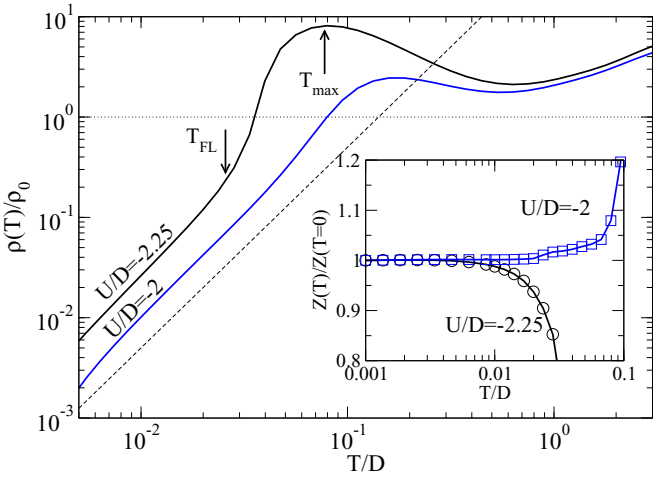

FIG. 9. (Color online) Resistivity on the log-log scale for attractive U near the localization transition. The dashed line has slope 2, expected for the Fermi-liquid regime. The dotted horizontal line indicates the Mott-Ioffe-Regel limit. For $U/D = -2.25$, two characteristic energy scales can be defined: the Fermi-liquid temperature $T_{\rm FL}$ and the resistivity peak temperature $T_{\max}$. Inset: rescaled quasiparticle renormalization factor $Z(T)/Z(T=0)$. Deviation from 1 indicates the end of the Landau Fermi-liquid regime.

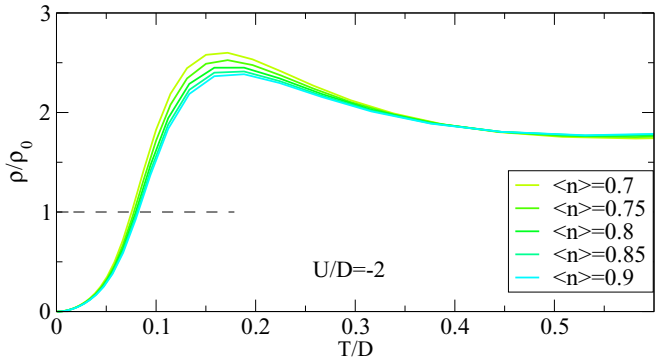

FIG. 10. (Color online) Resistivity at constant attractive U for a range of electron densities $\langle n \rangle$.

more negative for repulsive U and less negative for a range of attractive U. This behavior can be explained by the previously discussed asymmetry in the self-energy. On one hand, the contribution due to the transport function asymmetry is enhanced due to strong interactions (through a $1/Z$ factor), while the scattering rate asymmetry depends on the sign of U: for $U > 0$ it enhances the absolute value of S, while for $U < 0$ the two effects are antagonistic and $|S|$ is reduced. Some further details about the Seebeck coefficient and the role of the transport function $\Phi(\epsilon)$ are discussed in Sec. V C.

The temperature dependence of the thermopower is shown in Fig. 8(b). For positive U, the sign change of S reveals a change of the dominant transport mechanism and finds its counterpart in the kink in $\rho(T)$ [51]. For negative U, the Seebeck coefficient remains negative for all temperatures where reliable results can be obtained. At very low temperatures, it appears to become positive in a range of temperatures, but those results are uncertain. Further work with different numerical methods will be required to clarify the low-temperature behavior of the Seebeck coefficient in the attractive Hubbard model.

It is interesting to compare these findings for the attractive Hubbard model with those for the repulsive model at half-filling in the absence of the magnetic field (zero magnetization) [65]. The common feature is the nonmonotonic behavior of $\rho(T)$ and the resistivity peak much in excess of the MIR limit at the point where the quasiparticles are no longer present. The difference is found in the behavior of the thermopower. In the repulsive model it has a change of sign indicating the thermal destruction of the coherent Fermi-liquid state, similar to what is also found in doped Mott insulator (i.e., positive-U calculations at finite hole doping, as studied in this work and previously in Ref. [51]). In the attractive case, there is no such change of sign. This qualitative difference in the behavior of thermopower can be traced back to the partial particle-hole mapping [Eq. (4)], and its effect on the transport integrals. L_{jk} includes the factor

$$A_{\epsilon,\uparrow}(\omega)^2 + A_{\epsilon,\downarrow}(\omega)^2, \tag{14}$$

which maps to

$$A_{\epsilon,\uparrow}(\omega)^2 + A_{\epsilon,\downarrow}(-\omega)^2. \tag{15}$$

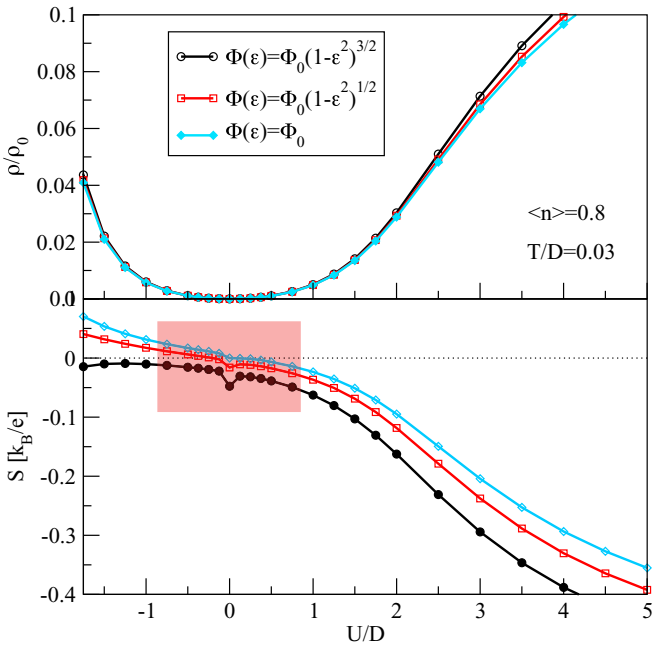

FIG. 11. (Color online) Resistivity and Seebeck coefficient at $T/D = 0.03$ for three choices of the transport function Φ. The data for the Seebeck coefficient in the shaded rectangle are not reliable for reasons explained in the text.

For spin down, the occupied and nonoccupied states in the spectral function are thus interchanged. This mostly affects L_{12} where the integrand is odd in ω and thus sensitive to the asymmetry of spectral functions.

C. Particle-hole asymmetry of the self-energy and the effect of different transport functions

We now provide some further details on the dependence of the numerical results for the transport properties on the choice of the transport function Φ [62,64]. Some common choices are

$\Phi_1(\epsilon) = \Phi_0[1 - (\epsilon/D)^2]^{3/2}$,
$\Phi_2(\epsilon) = \Phi_0[1 - (\epsilon/D)^2]^{1/2}$, and
$\Phi_3(\epsilon) = \Phi_0$.

In Fig. 11 the results for these three cases are plotted as a function of U for a fixed temperature $T/D = 0.03$. At this moderate temperature, the system is still in the Fermi-liquid regime for all values of U shown in the plot, yet the temperature is sufficiently high so that the causality-violation issues in the NRG do not affect the results except for a range of small U, where the oscillatory features in $\Sigma(\omega)$ are not much smaller than $|\mathrm{Im}\Sigma(\omega)|$ in the relevant frequency interval $\omega \in [-5T : 5T]$ (this is a well-known deficiency of the NRG). In addition, for two values of U we plot the temperature dependence of the Seebeck coefficient in Fig. 12.

The resistivity depends little on the choice of Φ (see top panel in Fig. 11). In the low-temperature limit, only the value of Φ at the Fermi level matters; it enters as a factor in the Fermi-liquid expression for the resistivity:

$$\rho(T) \propto \frac{1}{Z^2 \Phi(\epsilon_F)} T^2, \tag{16}$$

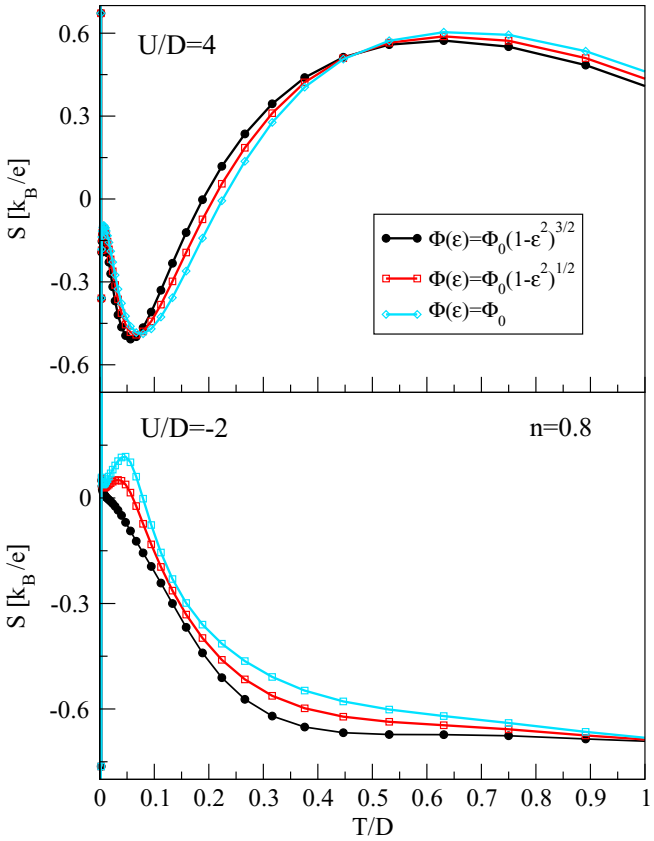

FIG. 12. (Color online) Seebeck coefficient vs temperature for two values of U, one positive (top panel) and one negative (bottom panel), for three choices of the transport function Φ. The two values are chosen so that they correspond to a comparable value of the quasiparticle renormalization factor Z. The results for $T/D \lesssim 0.01$ are not correct (note, for example, the downturn of S for $U/D = 4$ instead of linear low-temperature behavior).

where ϵ_F corresponds to the Fermi-surface value $\epsilon_F = \mu - \mathrm{Re}\Sigma(\omega = 0)$. Note that ϵ_F does not depend on U due to Luttinger's theorem, thus the value of the prefactor related to Φ is the same for all U. Even at higher temperatures beyond the Fermi-liquid regime, we find that the difference is only quantitative.

The Seebeck coefficient S is more subtle. For repulsive U, the difference is quantitative; when S is plotted as a function of the temperature, the effect of different Φ is mainly a slight shift of the characteristic temperatures (positions of extrema and zero crossings), but it hardly affects the overall scale of S (in particular the values at the minima and maxima) (see Fig. 12, top panel). This is not the case for attractive U, where we observe *qualitatively different* behavior at low temperatures: the sign itself of the low-temperature slope of the Seebeck coefficient depends on the choice of Φ (see Fig. 12, bottom panel).

As first pointed out by Haule and Kotliar [66], the particle-hole asymmetry terms in the low-frequency expansion of $\mathrm{Im}\Sigma$ may change the slope of $S(T)$ compared to the Fermi-liquid estimate which retains only the lowest-order $\omega^2 + (\pi k_B T)^2$ terms [51]. The full expression for the Seebeck coefficient in the low-temperature limit is [66]

$$S = -\frac{k_B}{e_0}\frac{k_B T}{Z}\left(\frac{E_2^1}{E_0^1}\frac{\Phi'(\epsilon_F)}{\Phi(\epsilon_F)} - \frac{a_1 E_4^2 + a_2 E_2^2}{\pi^2 \gamma_0 E_0^1}\right), \tag{17}$$

where E_n^k are numerical constants of order unity defined as

$$E_n^k = \int dx \frac{x^n}{\cosh(x/2)^2}\frac{1}{(1 + x^2/\pi^2)^k}, \tag{18}$$

a_i are the expansion coefficients of the cubic self-energy terms:

$$\Sigma^{(3)}(\omega) = \frac{a_1\omega^3 + a_2\omega T^2}{Z^3}, \tag{19}$$

and γ_0 is defined as the prefactor of the quadratic terms:

$$\Sigma^{(2)}(\omega) = \frac{\gamma_0}{Z^2}\left(\omega^2 + \pi^2 k_B^2 T^2\right). \tag{20}$$

The first term in Eq. (17) describes the particle-hole asymmetry in the electronic velocities, the second the asymmetry in the scattering rate. For fixed n, $\Phi'(\epsilon_F)/\Phi(\epsilon_F)$ is a fixed value that depends only on the choice of the function Φ. It is zero for $\Phi(\epsilon) = \text{const}$, and it differs by a factor of 3 for $\Phi(\epsilon) = \Phi_0(1 - \epsilon^2)^{1/2}$, where

$$\frac{\Phi'(\epsilon_F)}{\Phi(\epsilon_F)} = -\frac{\epsilon_F}{1 - \epsilon_F^2}, \tag{21}$$

and $\Phi(\epsilon) = \Phi_0(1 - \epsilon^2)^{3/2}$, where

$$\frac{\Phi'(\epsilon_F)}{\Phi(\epsilon_F)} = -\frac{3\epsilon_F}{1 - \epsilon_F^2}. \tag{22}$$

For different choices of Φ, the contribution of the first term in Eq. (17) forms a progression 0,1,3, which thus forms a gauge to assess its importance compared to the second term.

In Ref. [51], it was shown that for repulsive $U/D = 4$ the particle-hole asymmetry in the self-energy leads to a change of slope by a factor of more than 2. The rather small dependence of the slope of $S(T)$ on the choice of Φ seen in Fig. 12, top panel, actually suggests that the particle-hole asymmetry of $\mathrm{Im}\Sigma(\omega)$ is the *dominant contribution to the thermopower* for large U.

For attractive $U/D = -2$, the situation is even more interesting. Due to the asymmetry with long-lived hole states (see Fig. 6), the second term in Eq. (17) has a different sign from the first one. Since, in addition, the two terms are of similar magnitude, even the *sign of the slope* is affected by the choice of Φ.

Of course, for a real lattice the transport function Φ is fully determined by the dispersion relation and there is no element of indeterminacy. Nevertheless, the foregoing analysis has shown that the asymmetry term can be as large as or even larger than the first lowest-order Fermi-liquid term, possibly reversing the sign of the Seebeck coefficient. Proper inclusion of corrections to the Fermi-liquid theory are thus crucially (i.e., qualitatively) important for hole-doped systems with long-lived resilient quasihole states and electron-doped ones with long-lived quasiparticle states, and quantitatively important in general.

VI. OPTICAL CONDUCTIVITY

For both signs of U, the optical conductivity at low temperatures shows the well-known characteristics of the Fermi-liquid state in the Hubbard model [23,57]: a pronounced Drude peak at $\Omega = 0$ due to transitions inside the QP band, peak(s) or a band corresponding to transition between the QP band and the Hubbard bands near $\Omega = |U|/2$ or up to $\Omega \sim D$ (mid-infrared region), and a more diffuse peak at $\Omega = |U|$ due to the inter-Hubbard-band excitations. The results for attractive interaction $U/D = -2.25$ are shown in Fig. 13. At low temperatures, the peaks are rather well defined and clearly separated. As the temperature increases, the Drude peak intensity decreases. For $T \gtrsim T_{\mathrm{FL}}$, the intensity of the peak at $\Omega \approx |U|/2$ also drops and shifts toward lower frequencies. In this temperature range of $T \lesssim T_{\max}$, the optical spectral weight is transferred mostly to the $\Omega = |U|$ inter-Hubbard-band peak. As the temperature is increased further to $T \gtrsim T_{\max}$, there is a spectral redistribution in the opposite direction, from the $\Omega = |U|$ region to low-frequency regions, which corresponds to the decreasing dc resistivity in the temperature interval from $T_{\max}$ to the plateau of nearly constant resistivity around $T = 0.5D$, as seen in Figs. 7 and 8. (For the repulsive case, the temperature dependence of σ was studied in Ref. [51].)

For completeness, we also study the n dependence of the optical conductivity at two characteristic temperature regimes ($T/D = 10^{-2}$ is well in the Fermi-liquid regime, $T/D = 10^{-1}$ corresponds to the crossover regime between the low- and high-temperature asymptotics) for both signs of U (see Fig. 14).

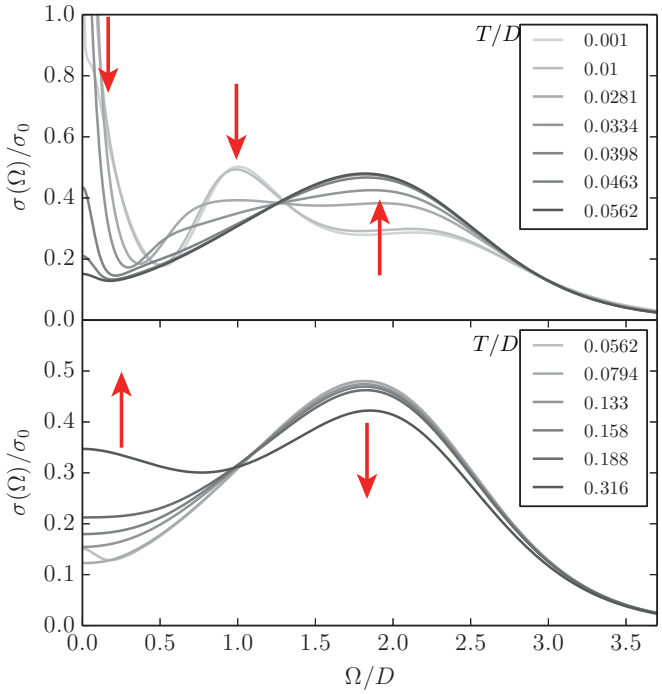

FIG. 13. (Color online) Optical conductivity for attractive $U/D = -2.25$ for a range of temperatures. The arrows indicate the evolution with increasing temperature in different frequency regions. Upper panel roughly corresponds to $T \lesssim T_{\max}$, lower to $T \gtrsim T_{\max}$.

For positive U, the results for the lower temperature $T/D = 10^{-2}$ (bottom right panel in Fig. 14) are easy to understand. With increasing doping (decreasing n), both Hubbard bands shift to higher energies, thus the corresponding optical peaks also move up. At the same time, the spectral weight of the QP band is increasing, while that of the Hubbard bands is decreasing; the system is becoming less correlated. This is reflected in the decreasing weight of the optical peak at $\Omega \approx U$ (upper Hubbard band, UHB), although that at $\Omega \approx 0.5D$ (lower Hubbard band, LHB) is actually increasing due to the increasing density of initial QP states. At the higher temperature $T/D = 10^{-1}$ (upper right panel in Fig. 14), the QP-LHB transitions can no longer be resolved, but the general trend with increasing doping is similar as in the Fermi-liquid regime.

For strong attraction, the optical conductivity is expected to weakly depend on doping since in the effective model, the changing magnetization leads to a rather moderate spectral weight redistribution: it mostly affects the total weight in the atomic peaks, while their positions remain essentially the same. The results are in agreement with the trends in the dc resistivity, shown in Fig. 10. The most significant variation of the dc resistivity is found in the peak region from $T \approx 0.1D$ to $0.2D$: in this temperature range, the optical conductivity is affected on an extended frequency range from $\Omega = 0$ up to $\Omega \approx 2D$ which includes the transitions inside the QP band and between the QP band and either Hubbard band: the main effect is that with increasing doping the optical conductivity decreases almost uniformly, with no changes in peak positions (upper left panel in Fig. 14). The behavior is different at the lower temperature of $T = 0.01D$ (bottom left panel in Fig. 14): the main effect there is a shift in the upper flank of the peak in $\sigma(\Omega)$ at $\Omega \approx |U|/2$, which corresponds to the transitions between the QP band and either Hubbard band, but little overall decrease in the optical conductivity.

VII. SPIN-LATTICE RELAXATION RATE AND DYNAMICAL SUSCEPTIBILITIES

The spin susceptibility can be probed in nuclear magnetic resonance (NMR) experiments. The spin-lattice relaxation rate $1/T_1$ quantifies the decay of the nuclear magnetic moments and provides information about the fluctuations of the electronic magnetic moments:

$$\frac{1}{T_1} = 2k_B T \left(\frac{g_N \mu_N}{g \mu_B}\right)^2 \sum_q |H_{\mathrm{hf}}(q)|^2 \mathrm{Im}\left[\frac{\chi^{+-}(q,\omega_N)}{\omega_N}\right], \tag{23}$$

where ω_N is the nuclear Larmor frequency which may be set to zero. If the hyperfine interaction $H_{\mathrm{hf}}(q)$ is local (i.e., has very weak q dependence), we are effectively probing the local dynamical magnetic susceptibility that is easily computed using the NRG. Furthermore, if there is no magnetic order, $\chi_{zz} = \frac{1}{2}\chi_{+-}$ due to isotropy in spin space. Thus, in the context of paramagnetic DMFT calculations, $1/T_1T$ measures the slope of the imaginary part of χ_{loc} in the zero-frequency limit.

The temperature dependence of the relaxation rate is shown in Fig. 15(a), where we plot the zero-frequency slope of the dynamical magnetic susceptibility (i.e., $1/T_1T$), and Fig. 15(c),

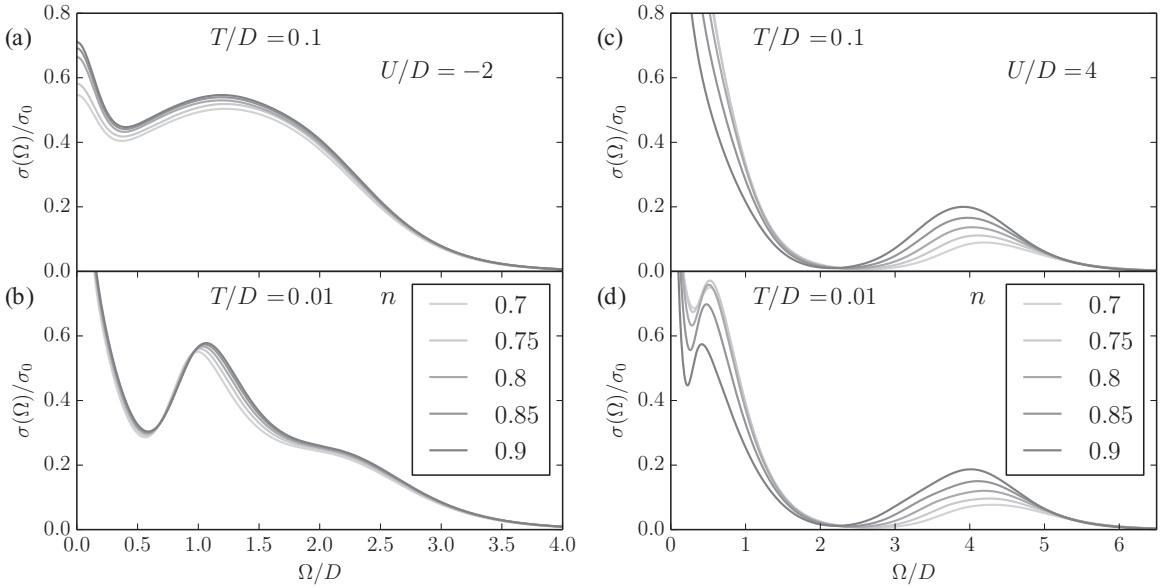

FIG. 14. Optical conductivity for $U/D = -2$ (left) and $U/D = 4$ (right) for a range of band fillings n.

where this same quantity is multiplied by the temperature (i.e., $1/T_1$). For strongly repulsive interaction, the relaxation rate $1/T_1T$ is monotonously decreasing with temperature: for $U/D = 4$ it drops by four orders of magnitude when going from $T = 0$ to $T \sim D$. For attractive U, the dependence is more complex and nonmonotonous. The case of $U/D = -2$ is typical for the strongly attractive regime. The pronounced minimum at $T \sim 0.1D$ corresponds to the maximum in $P_2(T) = \langle n_\uparrow n_\downarrow \rangle(T)$ [see Fig. 15(b)]: higher double occupancy (pairing) implies less-developed local moments. In the repulsive case, the behavior is opposite: P_2 starts by decreasing upon heating leading. In both cases, this leads to increased localization, which can be explained by the higher entropy in the Mott insulating (respectively pairing) phase [23]. We also generally observe that the scale of temperature variations is significantly smaller in the $U < 0$ case as compared to the $U > 0$ case. The presentation of the results as $1/T_1$ in Fig. 15(c) indicates the low-temperature metallic behavior (proportional to T) and regions of insulatorlike behavior with nearly constant $1/T_1$ (in particular, the bad-metal regime for large repulsive U).

The relaxation rate at $T = 0$ is plotted in Fig. 15(d). The general trend is expected: for the repulsive U the system

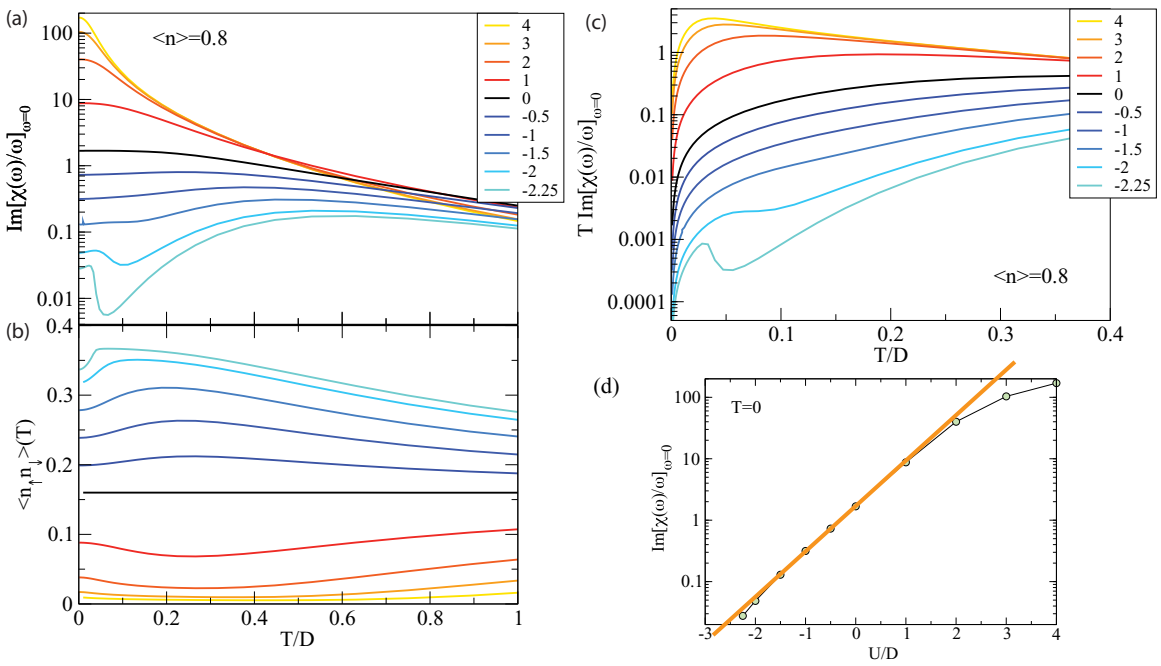

FIG. 15. (Color online) (a) Zero-frequency slope of the imaginary part of the local dynamical spin susceptibility, i.e., $1/T_1T$ up to constant prefactor. (b) Double occupancy as a function of temperature. (c) Zero-frequency slope multiplied by the temperature, i.e., $1/T_1$. (d) Zero-temperature spin relaxation rate vs Hubbard parameter U. The legends in (a) and (b) show the value of U/D.

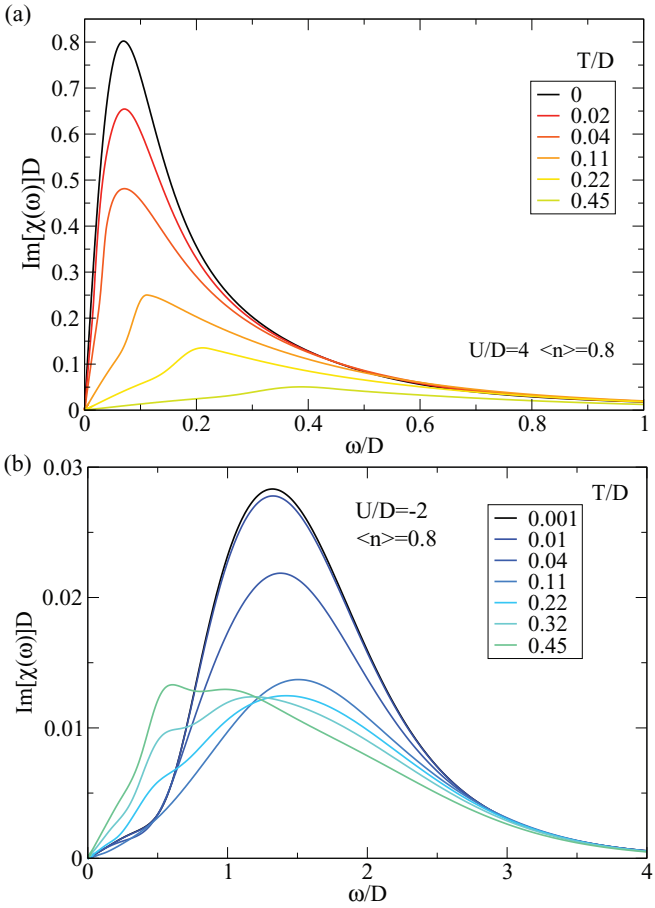

FIG. 16. (Color online) Imaginary part of the dynamical spin susceptibility for a range of temperatures for (a) repulsive interaction and (b) attractive interaction.

exhibits sizable magnetic fluctuations which saturate in the large-U limit, while for the attractive U the spin fluctuations rapidly freeze-out. In the interval $-D < U < D$, $1/T_1T$ depends exponentially on U, approximately as

$$\frac{1}{T_1T} \propto \exp\left(d\frac{U}{D}\right), \quad \text{with} \quad d \approx 1.7. \tag{24}$$

For a more strongly attractive U, the reduction becomes even more pronounced. This is associated with the emergence of the sharp Kondo resonance in the charge sector, while the spin fluctuations become negligible.

In Fig. 16, we show local dynamical spin susceptibility for a range of temperatures, one set for a representative case of repulsive (top panel) and one for attractive interaction (bottom panel). For $U/D = 4$, the dominant peak is on the Kondo scale with a maximum close to $\omega_{\rm sf} \approx 0.3ZD \approx 0.07$; this corresponds to the coherence scale of the problem [23]. This peak corresponds to the fluctuations of the local moments which is screened in the lattice version of the Kondo effect and is generated by the particle-hole excitations in the quasiparticle band. A much weaker peak (off scale in the plot) is present on the scale of charge fluctuations at $\omega \approx U$ due to particle-hole excitations with the hole in the LHB and the particle in the UHB. For temperatures below $T_{\rm coh} \approx \omega_{\rm sf}$, the susceptibility peak maximum remains close to $\omega_{\rm sf}$, only its amplitude is

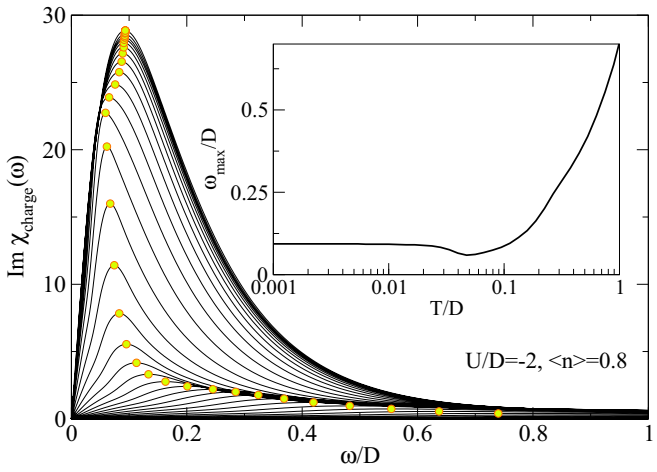

FIG. 17. (Color online) Dynamical charge susceptibility of the attractive Hubbard model for a range of temperatures. The insets shows the frequency of the peak as a function of the temperature.

decreasing with increasing temperature. For $T \gtrsim T_{\rm coh}$, the peak maximum itself shifts to higher frequencies; in fact, in this temperature regime the maximum occurs at $\omega \approx T$.

In the repulsive case, the spin fluctuations are expectedly much weaker. At $T = 0$, there is a single peak on the scale of $\omega \sim D$ and some nontrivial structure on the low-frequency scale of $\sim ZD$. The temperature variation is quite complex. Regime 1: Up to $T/D \sim 0.04$, the main effect is some reduction of weight in the high-frequency region, while the low-frequency region that determines $1/T_1$ is largely unaffected. Regime 2: For T/D between $\approx$0.04 and $\approx$0.11, there is a reduction of spin fluctuations on all energy scales, which corresponds to decreasing $1/T_1T$. Regime 3: For $T/D > 0.11$, a new peak starts to develop in the low-frequency region, while the high-energy peak shifts to lower frequencies; the two peaks merge at very high temperatures of order bandwidth. The crossovers between the regimes find their counterparts in the temperature dependence of the entropy (see Fig. 2). The crossover between regimes 1 and 2 corresponds to the emergence of an entropy plateau due to increasing pairing between the electrons. These pairs would condense into a coherent superconducting state if the superconducting order were allowed in our calculations. This crossover is not visible, however, in the transport properties: the resistivity is almost perfectly quadratic in both regimes 1 and 2 with no visible kinks (see Fig. 9). The crossover between regimes 2 and 3 can be interpreted as a thermal decomposition of the electron pairs. These regimes can also be observed in the dynamical charge susceptibility shown in Fig. 17. For $U < 0$, this quantity behaves somewhat similarly to the dynamical spin susceptibility for $U > 0$, except for a softening of the charge fluctuation mode in the temperature range between regimes 1 and 2 (the position of the peak versus T is shown in the inset).

The fine details in the dynamical susceptibility curves for $\omega \lesssim T$ should be interpreted with care due to possible artifacts [67]. In this respect, two-particle properties are even more challenging to determine reliably in the NRG at finite T than the single-particle properties. In particular, it is difficult to answer the question if a zero-frequency δ

peak is present in the greater Green's function $\mathrm{Im}\chi^{>}(\omega)$ at $T > 0$ as might be expected for unscreened local moments in the bad-metal regime of a doped Mott insulator. We indeed observe a δ peak develop as T is increased, but it can be shown that due to the particular way the spectra are computed in the NRG, some part of its weight is likely to be unphysical (see Appendix). Unfortunately, it is unclear how to separate the two contributions. In spite of these difficulties, the spin-lattice relaxation rate $1/T_1$ can be extracted relatively robustly from the retarded Green's function $\mathrm{Im}\chi(\omega)$ after spectral broadening with a kernel of width $\sim T$ and performing a linear fit in an interval of width $\Delta\omega \sim T$ around $\omega = 0$.

VIII. DISCUSSION: ANDERSON IMPURITY AT CONSTANT MAGNETIZATION

The nonmonotonic temperature dependencies in the attractive-U Hubbard model have been explained through the nontrivial properties of the positive-U model in magnetic field at constant magnetization. In this section, we investigate to what extent this behavior is present already at the level of the quantum impurity model without the self-consistency loop. In other words, we consider the Anderson impurity model at the particle-hole-symmetric point as a function of the external magnetic field B and the temperature T, and study its properties along the constant magnetization contours. The magnetic field is expressed in energy units (i.e., it includes the $g\mu_B$ prefactor, where g is the g factor and μ_B the Bohr magneton). We choose $U/D = 0.5$, $\delta = 0$ and a flat band with constant hybridization function $\Gamma/D = 0.05$. For this parameter set, the Kondo temperature according to Wilson's definition is $T_K/D = 10^{-3}$. We consider a temperature range up to $T = 0.05D = 50T_K$, where the Kondo peak is already strongly suppressed (but *still visible as a small hump* at the Fermi level), and magnetic fields up to $B = 0.02D = 20T_K$, where the spin polarization at low temperatures is 80% and there is a strong Kondo peak splitting (although the Zeeman-split peaks are *still clearly present*). The persistence of nontrivial low-frequency spectral features at T and B of several tens of T_K are worth stressing again: the Kondo effect is a crossover with logarithmic dependencies, thus it affects the system properties in a *wide temperature and field range much above the T_K scale*. This has obvious implications for the physics of the Hubbard model considered within the DMFT approach since a quasiparticle band must consequently be present on temperature scales much above $Z \sim T_K$, unless suppressed through the additional effect of the DMFT self-consistency constraint.

In Fig. 18(a), we plot the constant-magnetization contours in the (T, B) plane. For low magnetization, the contours are almost linear: curvature is visible only at low temperatures and high fields. We note that the attractive Hubbard model at $\langle n \rangle = 0.8$, the case we focused on in this work, corresponds to the $S_z = 0.1$ line; it is nearly perfectly linear for $T > T_K$ and has some weak curvature much below T_K. The impurity is best characterized by its thermodynamic properties, defined as the impurity contributions to the total quantities. In Figs. 18(b)–18(d) we show the results for spin and charge susceptibility, and the entropy in the (T, B) plane, while Fig. 18(e) presents the spin susceptibility along a set of constant-magnetization contours. We observe that there are no sharp features in any of these results: the crossovers are all smooth, with no visible kinks. This should be compared with the μ versus T curves for the attractive Hubbard model presented in Fig. 2, where

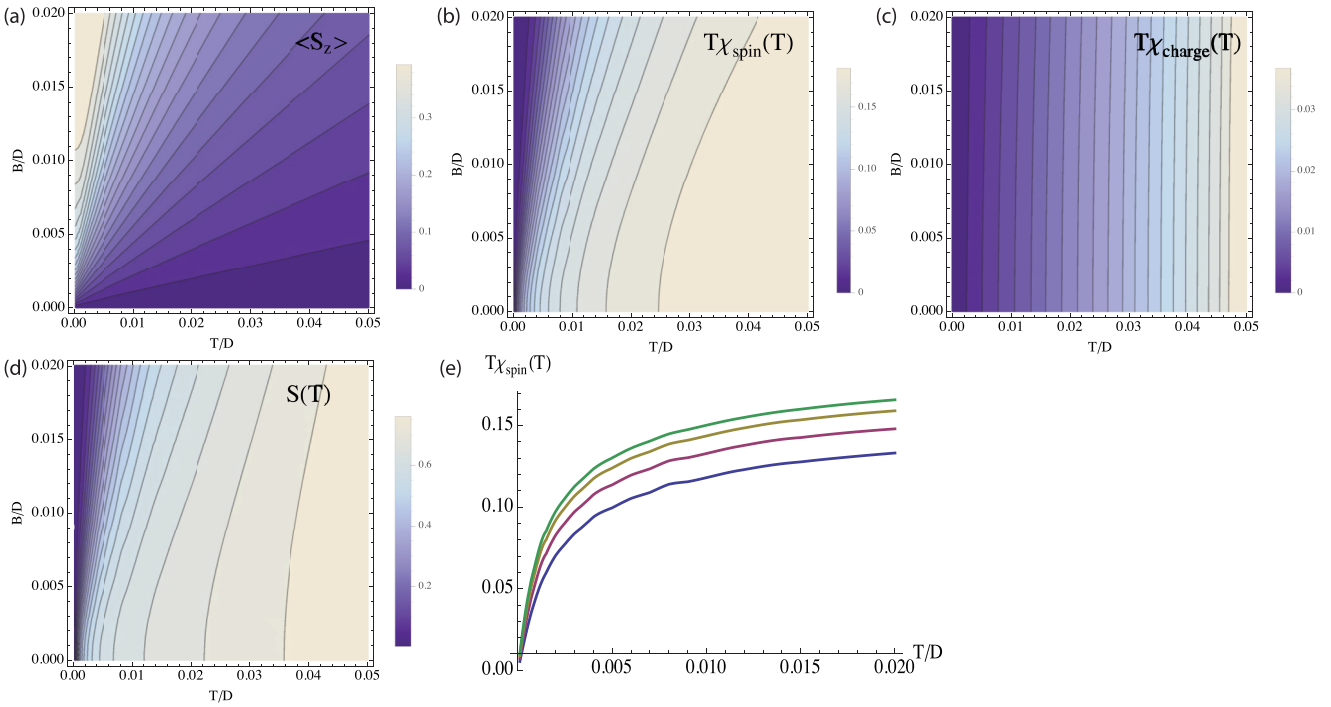

FIG. 18. (Color online) Properties of the single-impurity Anderson model at half-filling as a function of the temperature T and the magnetic field B. (a) Magnetization, (b) impurity spin susceptibility, (c) impurity charge susceptibility, and (d) impurity entropy. (e) Temperature dependence of the impurity spin susceptibility evaluated along the constant-magnetization contours (top to bottom: $\langle S_z \rangle = 0.05, 0.1, 0.1, 0.2$).

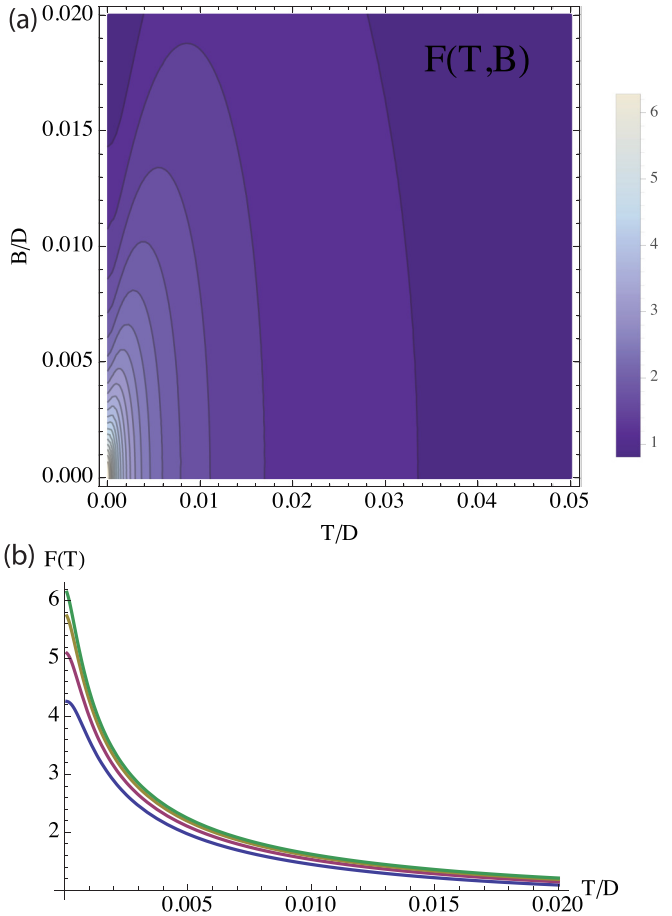

FIG. 19. (Color online) Conductivity $F(T,B)$ for a single-spin species in the single-impurity Anderson model at half-filling in external magnetic field (see the text for the exact definition). (a) Contour plot in the (T,B) plane. (b) Temperature dependence of the conductivity along the constant-magnetization contours (top to bottom: $\langle S_z \rangle = 0.05, 0.1, 0.15, 0.2$).

a kink becomes noticeable for sufficiently negative U. Such kinks must thus be generated through the self-consistency loop and are a genuine lattice effect that is not present at the single-impurity level. The susceptibility curves in Fig. 18(e) indicate that the crossover scale does not depend much on the magnetization. This property of the pure impurity model explains the results for the resistivity of the Hubbard model shown in Fig. 10 which indicate an analogous lack of dependence on the band filling.

In Fig. 19(a), we show the temperature and field dependence of the "conductivity" for a single-spin species of the symmetric Anderson impurity model as a function of temperature and magnetic field. The quantity shown is

$$F(T,B) = \int A_\sigma(\omega) \frac{\beta}{4\cosh(\beta\omega/2)} d\omega, \qquad (25)$$

i.e., the spin-resolved spectral function integrated with a thermal broadening kernel. A single-spin component is considered because under the partial particle-hole transformation, the original $U < 0$ spectral functions for *both* spins map to a single-spin-resolved function of the $U > 0$ model (this is strictly true at the particle-hole-symmetric point). The thermal kernel is the same as in the bulk expression for the dc conductivity [Eq. (10) in the $\Omega \to 0$ limit]. If the quantity $F(T,B)$ is evaluated along the constant-magnetization contours, we obtain the results shown in Fig. 19(b): the conductivity is monotonically decreasing, thus this simple calculation does not explain the nonmonotonous transport properties of the bulk attractive-U Hubbard model.

One final remark is in order. Figure 18 indicates that there is nothing special about the zero-magnetization line at $B = 0$ and that the results along the zero-magnetization contour do not differ drastically from those for finite-magnetization lines. This simply shows that as the doping in the attractive-U Hubbard model is reduced toward zero, the results are smoothly connected with those for the repulsive-U Hubbard model at half-filling in the absence of the field, except for the effects of the mapping of spectral functions [Eq. (4)] on the transport properties, in particular the thermopower, as already commented above [Eqs. (14) and (15)].

IX. EXPERIMENTAL RELEVANCE

A. Zeolites

Zeolites are aluminosilicate materials with microporous structure consisting of cages or channels with large voids which can accommodate alkali cations. They show a variety of exotic electronic properties, including different magnetically ordered states [68,69] and metal-insulator transitions [69]. The s electrons of alkali atoms are believed to be confined in the cages and the concentration of dopants strongly affects the electronic properties since it changes not only the band filling, but also the electronic potential depth, thereby controlling the electron-electron repulsion. Furthermore, the cations can undergo large displacements, thus there is significant electron-phonon coupling leading to polaron effects [69,70]. The appropriate model for such systems is thus some multiorbital variant of the Hubbard-Holstein model which takes into account the large number of electron orbitals inside the cages, and their consecutive filling as the concentration of dopant atoms is increased. The minimal model, however, is the single-orbital Hubbard-Holstein model, which may be expected to describe at least qualitatively the electrons in the topmost electronic band near the Fermi level. A detailed study of this model is beyond the scope of this work. Nevertheless, the Hubbard-Holstein model maps in the antiadiabatic limit onto the Hubbard model with effective interaction U_{eff} that depends on the original electron-electron repulsion U and on the value of the electron-phonon coupling g, thus some features of interest can be studied in this setting.

A question of direct experimental relevance is how the evolution of the two key parameters, the band occupancy n and the coupling U, is reflected in measurable quantities. The optical conductivity for a range of n at constant U was already shown (Fig. 14) and here we provide the results for a range of U at constant n in Fig. 20. The calculations are again performed at $T/D = 0.01$ (left panels) and $T/D = 0.1$ (right panels); the lower value is representative of low-temperature measurements, and the higher one of those near room temperature. As expected, the variation as a function of U is much stronger than the dependence on n. It affects the optical conductivity

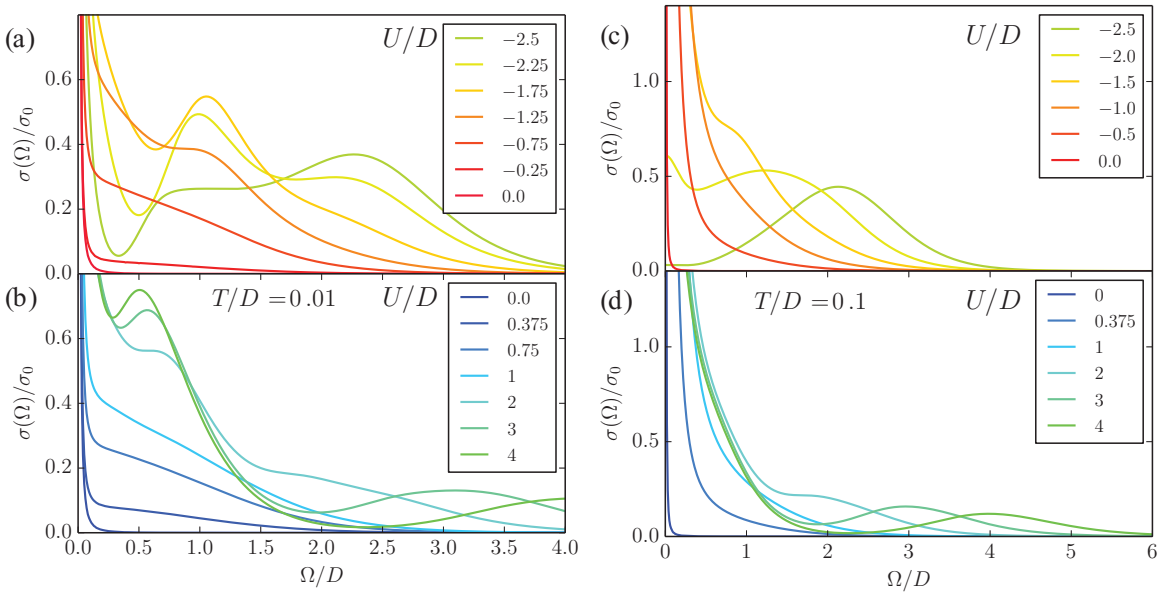

FIG. 20. (Color online) Optical conductivity for $n = 0.8$ for a range of repulsion parameters U. The finite width of the Drude peak for $U = 0$ is due to artificial broadening in the calculation. The absence of the Drude peak for $U/D = -2.5$ at $T/D = 0.1$ shows that the system is in the (bad) insulator regime.

on all frequency scales. At low U, the optical spectrum has a strong Drude peak with a "Drude foot" [71], but it is otherwise featureless; a well-defined structure becomes observable only for $|U| \gtrsim D$. Note that in the true Hubbard-Holstein model we expect a complex optical conductivity even for $U_{\text{eff}} = 0$ since the effective coupling is itself a frequency-dependent quantity.

B. Optical lattices

The results of this work are also directly relevant for the experiments on fermionic cold atoms confined in optical lattices [72]. The value and even the sign of the interparticle interaction can be tuned at will using the Feshbach resonances [73]. Since fermions are difficult to cool down to very low temperatures (below $0.1E_F$, where E_F is the Fermi energy), the ordered ground states (quantum magnetism) are not easy to reach [74]. For this reason, our results for the paramagnetic regime above ordering temperatures are actually precisely in the parameter range accessible to experiments. Recently, experiments aiming to measure the transport properties have been successfully performed [75,76]. Our results on the Hubbard model will become pertinent once similar experiments are performed on fermions in optical lattices. Such measurements should be able to detect the resistivity peak in excess of the MIR limit in the attractive-U case.

X. CONCLUSION

We have compared the basic properties of the Hubbard model constrained to the paramagnetic phase, with either repulsive or attractive electron-electron interactions for the same generic value of the occupancy $\langle n \rangle = 0.8$. The negative-U model can be understood in terms of the mapping via a partial particle-hole transformation to a positive-U model at half-filling in external magnetic field such that the magnetization is fixed to some constant value. This constraint leads to some interesting features. The resistivity in the attractive model strongly increases as the system approaches the transition to the pairing state (bipolaron formation). There would be phase separation, signaled in our calculations by the lack of convergence. The resistivity as a function of the temperature in the attractive model is nonmonotonous: it has a maximum on the scale $T_{\text{max}} = ZD$ where the quasiparticles disappear. The NMR relaxation rate in the attractive model has a complex nonmonotonic temperature dependence which reflects the nonmonotonic behavior of the double occupancy. Since strongly correlated metals with large electron-phonon coupling can have effective electron-electron interaction of either sign depending on the system parameters, our results provide some guidelines to distinguish the repulsive and attractive interactions in experiments.

ACKNOWLEDGMENTS

We acknowledge very useful discussions with J. Mravlje. R.Ž. and Ž.O. acknowledge the support of the Slovenian Research Agency (ARRS) under Program No. P1-0044.

APPENDIX: SPECTRAL SUM RULES IN THE NRG

In this Appendix, we discuss the spectral sum rules, the fluctuation-dissipation theorem, and the constraints to their applicability due to the nonexact nature of the NRG calculations, in particular at finite T, where the density-matrix NRG methods need to be used [77–80]. The Green's function associated with operators A and B is defined as [81]

$$G_{AB}(t) = -i\theta(t)\langle [A(t), B]_\epsilon \rangle, \tag{A1}$$

where $\epsilon = +1$ (anticommutator) if A and B are both fermionic, and $\epsilon = -1$ (commutator) otherwise. Furthermore, the

correlation functions are defined as

$$C^{>}_{AB}(t) = \langle A(t)B\rangle, \quad C^{<}_{AB}(t) = \langle BA(t)\rangle, \tag{A2}$$

and the lesser and greater Green's functions as

$$\begin{aligned} G^{>}_{AB}(t) &= -i\theta(t)\langle A(t)B\rangle, \\ G^{<}_{AB}(t) &= -i\theta(t)\epsilon\langle BA(t)\rangle. \end{aligned} \tag{A3}$$

The Fourier transforms are

$$C^{>,<}(\omega) = \int_{-\infty}^{\infty} dt\, e^{i\omega t} C^{>,<}(t), \tag{A4}$$

and the Laplace transform of the Green's functions ($z = \omega + i0^{+}$) is

$$G_{AB}(z) = \int_{0}^{\infty} dt\, e^{izt} G_{AB}(t). \tag{A5}$$

The relation between $C^{>,<}$ and $G^{<,>}$ is

$$\begin{aligned} [G^{>}_{AB}]''(\omega) &= -\pi C^{>}_{AB}(\omega), \\ [G^{<}_{AB}]''(\omega) &= -\pi\epsilon C^{<}_{AB}(\omega). \end{aligned} \tag{A6}$$

Here, $G''(\omega)$ denotes the jump function, which is here equal to the imaginary part of retarded Green's function, i.e., $\mathrm{Im}\, G(\omega + i\delta)$. The total spectral function can be written in several equivalent forms:

$$\begin{aligned} \rho_{AB}(\omega) &= C^{>}_{AB}(\omega) + \epsilon C^{<}_{AB}(\omega) \\ &= -\frac{1}{\pi}\{[G^{>}_{AB}]''(\omega + i0) + [G^{<}_{AB}]''(\omega + i0)\} \\ &= -\frac{1}{2\pi i}\left[G_{AB}(\omega + i0) - G_{AB}(\omega - i0)\right] \\ &= -\frac{1}{\pi} G''_{AB}(\omega + i0). \end{aligned} \tag{A7}$$

Using Lehmann's decomposition, one can show that

$$C^{>}_{AB}(\omega)e^{-\beta\omega} = C^{<}_{AB}(\omega), \tag{A8}$$

thus

$$C^{>}_{AB}(\omega) = \frac{G''_{AB}(\omega)}{1 + \epsilon e^{-\beta\omega}}. \tag{A9}$$

From this, one obtains

$$\langle A(t)B\rangle = \int_{-\infty}^{\infty} d\omega\, e^{-i\omega t} \frac{1}{\pi} \frac{G''_{AB}(\omega + i0)}{1 + \epsilon e^{-\beta\omega}}, \tag{A10}$$

and finally the fluctuation-dissipation theorem (FDT) in the form

$$\langle AB\rangle = \int_{-\infty}^{\infty} d\omega \frac{\rho_{AB}(\omega)}{1 + \epsilon e^{-\beta\omega}}. \tag{A11}$$

Alternatively, by integrating over the $C^{<,>}$ functions, one can obtain

$$\begin{aligned} \int_{-\infty}^{\infty} C^{>}_{AB}(\omega) d\omega &= \langle AB\rangle, \\ \int_{-\infty}^{\infty} C^{<}_{AB}(\omega) d\omega &= \langle BA\rangle. \end{aligned} \tag{A12}$$

It turns out that in the full-density-matrix numerical renormalization group (FDM-NRG), these two sum rules are satisfied exactly by construction (up to floating-point round-off errors of order 10^{-16}), as long as the expectation values on the right-hand side are evaluated using the suitable density-matrix aproach [80]. This is not the case, however, for the FDT in the form of Eq. (A11). It turns out that there is nothing in the NRG that guarantees that the detailed balance relation $C^{>}_{AB}(\omega)e^{-\beta\omega} = C^{<}_{AB}(\omega)$ [Eq. (A8)] should be fulfilled by construction. Greater and lesser correlation functions are calculated somewhat differently because in the FDM-NRG the expansions of the identity into kept and discarded states need to be performed differently in each case. In practice, at $T = 0$ the FDT from Eq. (A11) is fulfilled to numerical precision, but the error grows with increasing T. At very high temperature $T = 0.1D$, for example, the violation of the FDT is about one permil for the fermionic spectral function and a few percent for the dynamical spin susceptibility. This implies that the sum rules need to be checked at the level of $C^{>}$ and $C^{<}$ correlation functions.

[1] Leon N. Cooper, Bound electron pairs in a degenerate Fermi gas, Phys. Rev. **104**, 1189 (1956).

[2] J. Hubbard, Electron correlations in narrow energy bands, Proc. R. Soc. London, Ser. A **276**, 238 (1963).

[3] J. Kanamori, Electron correlation and ferromagnetism of transition metals, Prog. Theor. Phys. **30**, 275 (1963).

[4] M. C. Gutzwiller, Effect of correlation on the ferromagnetism of transition metals, Phys. Rev. Lett. **10**, 159 (1963).

[5] D. J. Scalapino, The case for $d_{x^2-y^2}$ pairing in the cuprate superconductors, Phys. Rep. **250**, 329 (1995).

[6] P. A. Lee, N. Nagaosa, and X.-G. Wen, Doping a Mott insulator: Physics of high-temperature superconductivity, Rev. Mod. Phys. **78**, 17 (2006).

[7] Adriana Moreo and D. J. Scalapino, Cold attractive spin polarized Fermi lattice gases and the doped positive U Hubbard model, Phys. Rev. Lett. **98**, 216402 (2007).

[8] L. Hackermüller, U. Schneider, M. Moreno-Cardoner, T. Kitagawa, T. Best, S. Will, E. Demler, E. Altman, I. Bloch, and B. Paredes, Anomalous expansion of attractively interacting fermionic atoms in an optical lattice, Science **327**, 1621 (2010).

[9] Ulrich Schneider, Lucia Hackermüller, Jens Philipp Ronzheimer, Sebastian Will, Simon Braun, Thorsten Best, Immanuel Bloch, Eugene Demler, Stephan Mandt, David Rasch, and Achim Rosch, Fermionic transport and out-of-equilibrium dynamics in a homogeneous Hubbard model with ultracold atoms, Nat. Phys. **8**, 213 (2012).

[10] R. Micnas, J. Ranninger, and S. Robaszkiewicz, Superconductivity in narrow-band systems with local non-retarded interactions, Rev. Mod. Phys. **62**, 113 (1990).

[11] M. Keller, W. Metzner, and U. Schollwöck, Dynamical mean-field theory for pairing and spin gap in the attractive Hubbard model, Phys. Rev. Lett. **86**, 4612 (2001).

[12] M. Capone, C. Castellani, and M. Grilli, First-order pairing transition and single-particle spectral function in the attractive Hubbard model, Phys. Rev. Lett. **88**, 126403 (2002).

[13] A. Toschi, P. Barone, M. Capone, and C. Castellani, Pairing and superconductivity from weak to strong coupling in the attractive Hubbard model, New J. Phys. **7**, 7 (2005).

[14] Chih-Chun Chien, Qijin Chen, and K. Levin, Fermions with attractive interactions on optical lattices and implications for correlated systems, Phys. Rev. A **78**, 043612 (2008).

[15] J. Bauer, A. C. Hewson, and N. Dupuis, DMFT-NRG for superconductivity in the attractive Hubbard model, Phys. Rev. B **79**, 214518 (2009).

[16] N. A. Kuleeva, E. Z. Kuchinskii, and M. V. Sadovskii, Normal phase and superconductivity in the attractive Hubbard model: A dmft(nrg) study, JETP **119**, 264 (2014).

[17] W. Koller, D. Meyer, and A. Hewson, Dynamic response functions for the Holstein-Hubbard model, Phys. Rev. B **70**, 155103 (2004).

[18] P. Paci, M. Capone, E. Cappelluti, S. Ciuchi, and C. Grimaldi, Isotope effects in the Hubbard-Holstein model within dynamical mean-field theory, Phys. Rev. B **74**, 205108 (2006).

[19] J Bauer, Competing interactions and symmetry breaking in the Hubbard-Holstein model, Europhys. Lett. **90**, 27002 (2010).

[20] Johannes Bauer and Alex C Hewson, Competition between antiferromagnetic and charge order in the Hubbard-Holstein model, Phys. Rev. B **81**, 235113 (2010).

[21] Antoine Georges, Condensed matter physics with light and atoms: Strongly correlated cold fermions in optical lattices, Lectures given at the Enrico Fermi Summer School on "Ultracold Fermi Gases," organized by M. Inguscio, W. Ketterle, and C. Salomon, Varenna, Italy, June 2006, arXiv:cond-mat/0702122v1.

[22] W. Metzner and D. Vollhardt, Correlated lattice fermions in $d = \infty$ dimensions, Phys. Rev. Lett. **62**, 324 (1989).

[23] Antoine Georges, Gabriel Kotliar, Werner Krauth, and Marcelo J. Rozenberg, Dynamical mean-field theory of strongly correlated fermion systems and the limit of infinite dimensions, Rev. Mod. Phys. **68**, 13 (1996).

[24] M. Jarrell, Hubbard model in infinite dimensions: A quantum Monte Carlo study, Phys. Rev. Lett. **69**, 168 (1992).

[25] A. Georges and W. Krauth, Physical properties of the half-filled Hubbard model in infinite dimensions, Phys. Rev. B **48**, 7167 (1993).

[26] M. J. Rozenberg, G. Kotliar, and X. Y. Zhang, Mott-Hubbard transition in infinite dimensions. II, Phys. Rev. B **49**, 10181 (1994).

[27] Akihisa Koga and Philipp Werner, Low-temperature properties of the infinite-dimensional attractive Hubbard model, Phys. Rev. A **84**, 023638 (2011).

[28] A Georges, Thinking locally: Reflections on dynamical mean-field theory from a high-temperature/high-energy perspective, Ann. Phys. (Leipzig) **523**, 672 (2011).

[29] E. Müller-Hartmann, Correlated fermions on a lattice in high dimensions, Z. Phys. B: Condens. Matter **74**, 507 (1989).

[30] Antoine Georges and Gabriel Kotliar, Hubbard model in infinite dimensions, Phys. Rev. B **45**, 6479 (1992).

[31] M. J. Rozenberg, X. Y. Zhang, and G. Kotliar, Mott-Hubbard transition in infinite dimensions, Phys. Rev. Lett. **69**, 1236 (1992).

[32] X. Y. Zhang, M. J. Rozenberg, and G. Kotliar, Mott transition in the $d = \infty$ Hubbard model at zero temperature, Phys. Rev. Lett. **70**, 1666 (1993).

[33] G. Kotliar, S. Y. Savrasov, K. Haule, V. S. Oudovenko, O. Parcollet, and C. A. Marianetti, Electronic structure calculations with dynamical mean-field theory, Rev. Mod. Phys. **78**, 865 (2006).

[34] K. G. Wilson, The renormalization group: Critical phenomena and the Kondo problem, Rev. Mod. Phys. **47**, 773 (1975).

[35] H. R. Krishna-murthy, J. W. Wilkins, and K. G. Wilson, Renormalization-group approach to the Anderson model of dilute magnetic alloys. I. static properties for the symmetric case, Phys. Rev. B **21**, 1003 (1980).

[36] O. Sakai, Y. Shimizu, and T. Kasuya, Single-particle and magnetic excitation spectra of degenerate Anderson model with finite f-f Coulomb interaction, J. Phys. Soc. Jpn. **58**, 3666 (1989).

[37] T. A. Costi, A. C. Hewson, and V. Zlatić, Transport coefficients of the Anderson model via the numerical renormalization group, J. Phys.: Condens. Matter **6**, 2519 (1994).

[38] R. Bulla, A. C. Hewson, and Th. Pruschke, Numerical renormalization group calculation for the self-energy of the impurity Anderson model, J. Phys.: Condens. Matter **10**, 8365 (1998).

[39] R. Bulla, Zero temperature metal-insulator transition in the infinite-dimensional Hubbard model, Phys. Rev. Lett. **83**, 136 (1999).

[40] Th. Pruschke, R. Bulla, and M. Jarrell, Low-energy scale of the periodic Anderson model, Phys. Rev. B **61**, 12799 (2000).

[41] Ralf Bulla, Theo Costi, and Thomas Pruschke, The numerical renormalization group method for quantum impurity systems, Rev. Mod. Phys. **80**, 395 (2008).

[42] Rok Žitko and Thomas Pruschke, Energy resolution and discretization artefacts in the numerical renormalization group, Phys. Rev. B **79**, 085106 (2009).

[43] H. O. Frota and L. N. Oliveira, Photoemission spectroscopy for the spin-degenerate Anderson model, Phys. Rev. B **33**, 7871 (1986).

[44] V. L. Campo and L. N. Oliveira, Alternative discretization in the numerical renormalization group, Phys. Rev. B **72**, 104432 (2005).

[45] Rok Žitko, Convergence acceleration and stabilization for dynamical-mean-field-theory calculations, Phys. Rev. B **80**, 125125 (2009).

[46] E. H. Lieb, Two theorems on the Hubbard model, Phys. Rev. Lett. **62**, 1201 (1989).

[47] L. Laloux, A. Georges, and W. Krauth, Effect of a magnetic field on Mott-Hubbard systems, Phys. Rev. B **50**, 3092 (1994).

[48] J. Bauer and A. C. Hewson, Field-dependent quasiparticles in the infinite-dimensional Hubbard model, Phys. Rev. B **76**, 035118 (2007).

[49] J. Bauer, Quasiparticle properties of strongly correlated electron systems with itinerant metamagnetic behavior, Eur. Phys. J. B **68**, 201 (2009).

[50] Rok Žitko, Janez Bonča, and Thomas Pruschke, Van Hove singularities in the paramagnetic phase of the Hubbard model: A DMFT study, Phys. Rev. B **80**, 245112 (2009).

[51] Xiaoyu Deng, Jernej Mravlje, Rok Žitko, Michel Ferrero, Gabriel Kotliar, and Antoine Georges, How bad metals turn good: Spectroscopic signatures of resilient quasiparticles, Phys. Rev. Lett. **110**, 086401 (2013).

[52] R. Žitko, D. Hansen, E. Perepelitsky, J. Mravlje, A. Georges, and B. S. Shastry, Extremely correlated Fermi liquid theory meets dynamical mean-field theory: Analytical insights into the doping-driven Mott transition, Phys. Rev. B **88**, 235132 (2013).

[53] A. C. Hewson, J. Bauer, and W. Koller, Field dependent quasiparticles in a strongly correlated local system, Phys. Rev. B **73**, 045117 (2006).

[54] Anil Khurana, Electrical conductivity in the infinite-dimensional Hubbard model, Phys. Rev. Lett. **64**, 1990 (1990).

[55] H. Schweitzer and G. Czycholl, Resistivity and thermopower of heavy-fermion systems, Phys. Rev. Lett. **67**, 3724 (1991).

[56] T. Pruschke, D. L. Cox, and M. Jarrell, Transport properties of the infinite dimensional Hubbard model, Europhys. Lett. **21**, 593 (1993).

[57] T. Pruschke, D. L. Cox, and M. Jarrell, Hubbard model at inifnite dimensions: Thermodynamics and transport properties, Phys. Rev. B **47**, 3553 (1993).

[58] T. Pruschke, M. Jarrell, and J. K. Freericks, Anomalous normal-state properties of high-tc superconductors: Intrinsic properties of strongly correlated electron systems? Adv. Phys. **44**, 187 (1995).

[59] M. Jarrell, J. K. Freericks, and Th. Pruschke, Optical conductivity of the infinite-dimensional Hubbard model, Phys. Rev. B **51**, 11704 (1995).

[60] M. J. Rozenberg, G. Kotliar, and H. Kajueter, Transfer of spectral weight in spectroscopies of correlated electron systems, Phys. Rev. B **54**, 8452 (1996).

[61] G. Pálsson, Computational studies of thermoelectricity in strongly correlated electron systems, Ph.D. thesis, Rutgers University, 2001.

[62] Nils Blümer, Mott-Hubbard Metal-Insulator Transition and Optical Conductivity in High Dimensions, Ph.D. thesis, University of Augsburg, 2002.

[63] Woonki Chung and J. K. Freericks, Charge-transfer metal-insulator transitions in the spin-1/2 Falicov-Kimball model, Phys. Rev. B **57**, 11955 (1998).

[64] L.-F. Arsenault and A.-M. S. Tremblay, Transport functions for hypercubic and Bethe lattices, Phys. Rev. B **88**, 205109 (2013).

[65] J. Merino and R. H. McKenzie, Transport properties of strongly correlated metals: A dynamical mean-field approach, Phys. Rev. B **61**, 7996 (2000).

[66] K. Haule and G. Kotliar, "Thermoelectrics near the Mott localization-delocalization transition, in *Properties and Applications of Thermoelectric Materials*, edited by V. Zlatić and A. C. Hewson (Springer, Dordrecht, 2009), p. 119.

[67] Žiga Osolin and Rok Žitko, Padé approximant approach for obtaining finite-temperature spectral functions of quantum impurity models using the numerical renormalization group technique, Phys. Rev. B **87**, 245135 (2013).

[68] Duong Thi Hanh, Takehito Nakano, and Yasuo Nozue, Strong dependence of ferrimagnetic properties on Na concentration in Na–K alloy clusters incorporated in low-silica X zeolite, J. Phys. Chem. Solids **71**, 677 (2014).

[69] Takehito Nakano, Duong Thi Hanh, Akihiro Owaki, Yasuo Nozue, Nguyen Hoang Nam, and Shingo Araki, Insulator-to-metal transition and magnetism of potassium metals loaded into regular cages of zeolite LSX, J. Korean Phys. Soc. **63**, 512 (2013).

[70] Mutsuo Igarashi, Takehito Nakano, Pham Thi, Yasuo Nozue, Atsushi Goto, Kenjiro Hashi, Shinobu Ohki, Tadashi Shimizu, Andraž Krajnc, Peter Jeglič, and Denis Arčon, NMR study of thermally activated paramagnetism in metallic low-silica X zeolite filled with sodium atoms, Phys. Rev. B **87**, 075138 (2013).

[71] C. Berthod, J. Mravlje, X. Deng, R. Žitko, D. van der Marel, and A. Georges, Non-Drude universal scaling laws for the optical response of local Fermi liquids, Phys. Rev. B **87**, 115109 (2013).

[72] Immanuel Bloch and Wilhelm Zwerger, Many-body physics with ultracold gases, Rev. Mod. Phys. **80**, 885 (2008).

[73] Cheng Chin, Paul Julienne, and Eite Tiesinga, Feshbach resonances in ultracold gases, Rev. Mod. Phys. **82**, 1225 (2010).

[74] D. Greif, T. Uehlinger, G. Jotzu, L. Tarruell, and T. Esslinger, Short-range quantum magnetism of ultracold fermions in an optical lattice, Science **340**, 1307 (2013).

[75] J. P. Brantut, J. Meineke, D. Stadler, S. Krinner, and T. Esslinger, Conduction of ultracold fermions through a mesoscopic channel, Science **337**, 1069 (2012).

[76] J. P. Brantut, C. Grenier, J. Meineke, D. Stadler, S. Krinner, C. Kollath, T. Esslinger, and A. Georges, A thermoelectric heat engine with ultracold atoms, Science **342**, 713 (2013).

[77] Walter Hofstetter, Generalized numerical renormalization group for dynamical quantities, Phys. Rev. Lett. **85**, 1508 (2000).

[78] F. B. Anders and A. Schiller, Real-time dynamics in quantum impurity systems: A time-dependent numerical renormalization group approach, Phys. Rev. Lett. **95**, 196801 (2005).

[79] Robert Peters, Thomas Pruschke, and Frithjof B. Anders, A numerical renormalization group approach to Green's functions for quantum impurity models, Phys. Rev. B **74**, 245114 (2006).

[80] Andreas Weichselbaum and Jan von Delft, Sum-rule conserving spectral functions from the numerical renormalization group, Phys. Rev. Lett. **99**, 076402 (2007).

[81] Th. Pruschke, "Vielteilchentheorie des Festkörpers", Lecture notes (unpublished).